



Chinese Pharmaceutical Association  
Institute of Materia Medica, Chinese Academy of Medical Sciences

Acta Pharmaceutica Sinica B

[www.elsevier.com/locate/apsb](http://www.elsevier.com/locate/apsb)  
[www.sciencedirect.com](http://www.sciencedirect.com)



ORIGINAL ARTICLE

# Rhizoma Drynariae-derived nanovesicles reverse osteoporosis by potentiating osteogenic differentiation of human bone marrow mesenchymal stem cells *via* targeting ER $\alpha$ signaling



Qing Zhao<sup>a,b,†</sup>, Junjie Feng<sup>c,d,†</sup>, Fubin Liu<sup>a,b,†</sup>, Qianxin Liang<sup>e</sup>,  
Manlin Xie<sup>a,b</sup>, Jiaming Dong<sup>a,b</sup>, Yanfang Zou<sup>a,b</sup>, Jiali Ye<sup>a,b</sup>,  
Guilong Liu<sup>a,b,f</sup>, Yue Cao<sup>a,b</sup>, Zhaodi Guo<sup>a,b</sup>, Hongzhi Qiao<sup>g,\*</sup>,  
Lei Zheng<sup>a,b,c,d,\*</sup>, Kewei Zhao<sup>a,b,\*</sup>

<sup>a</sup>Guangzhou Key Laboratory of Chinese Medicine Research on Prevention and Treatment of Osteoporosis, the Third Affiliated Hospital of Guangzhou University of Chinese Medicine, Guangzhou 510378, China

<sup>b</sup>Guangdong Engineering Research Center of Chinese Herbal-derived Vesicles, Guangzhou University of Chinese Medicine, Guangzhou 510006, China

<sup>c</sup>Department of Laboratory Medicine, Nanfang Hospital, Southern Medical University, Guangzhou 510515, China

<sup>d</sup>Guangdong Engineering and Technology Research Center for Rapid Diagnostic Biosensors, Nanfang Hospital, Southern Medical University, Guangzhou 510515, China

<sup>e</sup>The Fifth Affiliated Hospital Sun Yat-sen University, Zhuhai 519000, China

<sup>f</sup>Department of Blood Transfusion, Guangdong Heyou International Hospital, Foshan 528306, China

<sup>g</sup>School of Pharmacy, Nanjing University of Chinese Medicine, Nanjing 210023, China

Received 26 November 2023; received in revised form 27 December 2023; accepted 8 January 2024

## KEY WORDS

Rhizoma Drynariae-derived nanovesicles;

**Abstract** Although various anti-osteoporosis drugs are available, the limitations of these therapies, including drug resistance and collateral responses, require the development of novel anti-osteoporosis agents. Rhizoma Drynariae displays a promising anti-osteoporosis effect, while the effective component

\*Corresponding authors.

E-mail addresses: [qiaohz@njucm.edu.cn](mailto:qiaohz@njucm.edu.cn) (Hongzhi Qiao), [nfyyzhenglei@smu.edu.cn](mailto:nfyyzhenglei@smu.edu.cn) (Lei Zheng), [zkw2011@gzucm.edu.cn](mailto:zkw2011@gzucm.edu.cn) (Kewei Zhao).

<sup>†</sup>These authors made equal contributions to this work.

Peer review under the responsibility of Chinese Pharmaceutical Association and Institute of Materia Medica, Chinese Academy of Medical Sciences.

<https://doi.org/10.1016/j.apsb.2024.02.005>

2211-3835 © 2024 The Authors. Published by Elsevier B.V. on behalf of Chinese Pharmaceutical Association and Institute of Materia Medica, Chinese Academy of Medical Sciences. This is an open access article under the CC BY-NC-ND license (<http://creativecommons.org/licenses/by-nc-nd/4.0/>).

Bone marrow mesenchymal stem cells;  
 Bone targeting;  
 Osteogenic differentiation;  
 ER $\alpha$  signaling;  
 Naringin;  
 Bone morphogenetic protein 2;  
 Runt-related transcription factor 2

and mechanism remain unclear. Here, we revealed the therapeutic potential of Rhizoma Drynariae-derived nanovesicles (RDNVs) for postmenopausal osteoporosis and demonstrated that RDNVs potentiated osteogenic differentiation of human bone marrow mesenchymal stem cells (hBMSCs) by targeting estrogen receptor- $\alpha$  (ER $\alpha$ ). RDNVs, a natural product isolated from fresh Rhizoma Drynariae root juice by differential ultracentrifugation, exhibited potent bone tissue-targeting activity and anti-osteoporosis efficacy in an ovariectomized mouse model. RDNVs, effectively internalized by hBMSCs, enhanced proliferation and ER $\alpha$  expression levels of hBMSC, and promoted osteogenic differentiation and bone formation. Mechanistically, *via* the ER $\alpha$  signaling pathway, RDNVs facilitated mRNA and protein expression of bone morphogenetic protein 2 and runt-related transcription factor 2 in hBMSCs, which are involved in regulating osteogenic differentiation. Further analysis revealed that naringin, existing in RDNVs, was the active component targeting ER $\alpha$  in the osteogenic effect. Taken together, our study identified that naringin in RDNVs displays exciting bone tissue-targeting activity to reverse osteoporosis by promoting hBMSCs proliferation and osteogenic differentiation through estrogen-like effects.

© 2024 The Authors. Published by Elsevier B.V. on behalf of Chinese Pharmaceutical Association and Institute of Materia Medica, Chinese Academy of Medical Sciences. This is an open access article under the CC BY-NC-ND license (<http://creativecommons.org/licenses/by-nc-nd/4.0/>).

## 1. Introduction

Postmenopausal osteoporosis (PMOP) is caused by the loss of estrogen owing to the functional failure of ovaries<sup>1,2</sup>. Unbalanced bone homeostasis resulting from bone formation by osteoblasts and bone resorption by osteoclasts has been recognized as the major cause of osteoporosis<sup>3,4</sup>. Although diverse clinical drugs are available for osteoporosis therapy, the severe side effects limit their further promotion and application. For example, bisphosphonates, an osteoclast inhibitor, may cause excessive suppression of bone turnover, resulting in low trauma, atypical fractures, esophagitis, and atrial fibrillation<sup>5</sup>. Moreover, although estrogen replacement therapy has a good effect on preventing PMOP, it frequently increases the risk for endometrial, ovarian, and mammary carcinomas because of its powerful estrogenic activity<sup>6–8</sup>. Therefore, developing a new agent that potentiates bone formation is of great importance.

Cell-derived nanovesicles (NVs) with nano-size membranous structures transport biological information, including nucleic acid, proteins, lipids, and metabolites, which are transferred between different species and regulate the biological functions of the organism<sup>9–11</sup>. Recently, NVs secreted by mammalian cells have been widely exploited in various biomedical applications, including drug delivery, disease diagnosis, and tissue repair<sup>11–13</sup>. Interestingly, plant-derived NVs offer multiple benefits, including biocompatibility, cost-effectiveness, eco-friendliness, and large-scale production<sup>14,15</sup>. Recent studies indicated that plant-derived NVs may regulate plant innate immunity by plant cell–cell communication<sup>16</sup> or transfer cross-species small RNA interference, causing fungal pathogen gene silencing<sup>17</sup>. In addition, bioactive components contained in plant-derived NVs could greatly shape the gut microbiota in mice, prevent alcohol-induced liver damage, and treat inflammatory tumors *via* the oral route or tail vein injection<sup>18–20</sup>.

Rhizoma Drynariae, an herbal medicine with pain-relieving and bone-strengthening properties, is commonly used in the clinical treatment of bone-related diseases, including osteoporosis, bone nonunion, bone fractures, and joint diseases<sup>21,22</sup>. However, the problems of poor solubility and non-selective distribution of

active ingredients from traditional herbal medicines *in vivo* urgently needed to be solved<sup>23,24</sup>. Furthermore, the effective component of Rhizoma Drynariae in anti-osteoporosis and its function remain unknown. In recent years, based on their low immunogenicity, high productivity, and medicinal properties, fresh herb-derived NVs have been investigated as suitable carriers of natural active contents<sup>25</sup>. We have reported previously that Rhizoma Drynariae releases NVs<sup>26</sup>, but the physiological function of plant-derived NVs in mammalian cells remains unknown. Because the benefits of herb-derived NVs are mainly dependent on their bioactive ingredient<sup>27</sup>, it is reasonable to speculate that Rhizoma Drynariae-derived nanovesicles (RDNVs) are enriched with specific bio-functional molecules and could be employed as an appropriate theranostic nanoplatform.

Human bone marrow mesenchymal stem cells (hBMSCs) play a vital role in osteogenic differentiation and bone formation<sup>28–30</sup>. In particular, estrogen receptor- $\alpha$  (ER $\alpha$ ) is widely used as an important target of clinical drugs for osteoporosis treatment, including tamoxifen and raloxifene<sup>31</sup>. Interestingly, the osteogenic differentiation of hBMSCs is diminished in the presence of ER $\alpha$  inhibitor, while RDNVs could reverse this inhibitory effect. In the study, we demonstrated RDNVs isolated from fresh Rhizoma Drynariae to be an active ER $\alpha$  agonist. Furthermore, we revealed that RDNVs had a potent therapeutic effect on PMOP by inducing hBMSC osteogenic differentiation and bone formation. Moreover, we found that RDNVs target femur tissue but without organ toxicity. Importantly, through high-performance liquid chromatography (HPLC) verification and bioinformatics analysis, we demonstrated that naringin is a bioactive metabolite of RDNVs, and it activates ER $\alpha$  signaling by promoting the expression of bone morphogenetic protein 2 (BMP2) and runt-related transcription factor 2 (RUNX2) in hBMSCs, resulting in the activation of osteoblast formation (Fig. 1).

Here, we obtained the natural product RDNVs, isolated and purified from fresh Rhizoma Drynariae by differential hypervelocity centrifugation. Experiments *in vivo* indicated that RDNVs preferentially accumulated in femur tissues, increased bone mass, and contributed to an anti-PMOP effect. Then, through experiments *in vitro* and bioinformatics analysis such as molecular

docking, we revealed the underlying mechanism of the pro-osteogenic properties of naringin enriched in RDNVs *via* targeting of ER $\alpha$  signaling. Based on all of the above, the study contributes to the development of a novel nanotherapeutic platform for the treatment of PMOP *via* i.p. administration, which has a promising potential for clinical transformation.

## 2. Materials and methods

### 2.1. Materials

Fresh Rhizoma Drynariae roots were dug up from Zhaoqing City, Guangdong Province, China. The Bicinchoninic Acid (BCA) kit was purchased from Beyotime Biotechnology Co., Ltd. (Beijing, China). Exosome-specific lysing solution (UR33101) was from Umibio Science and Technology Group (Shanghai, China). ICI 182,780 was supplied by MilliporeSigma (Burlington, MA, USA). Cell Counting Kit 8 (CCK-8) reagent was obtained from Biosharp (Hefei, China). 1,1'-Dioctadecyl-3,3,3',3'-tetramethylindocarbocyanine perchlorate (DiI), 1,1'-dioctadecyl-3,3,3',3'-tetramethylindotricarbocyanine iodide (DiR) and TRIzol reagent were obtained from Invitrogen (Waltham, MA, USA). Hoechst was obtained from MedChemExpress (Monmouth Junction, NJ, USA). A rabbit polyclonal glyceraldehyde-3-phosphate dehydrogenase (GAPDH) antibody (abs132004) was purchased from Absin Bioscience (Shanghai, China). A rabbit polyclonal antibody against ER $\alpha$  was obtained from Santa Cruz Biotechnology (Dallas, TX, USA). Rabbit polyclonal antibodies against BMP2 ([EPR24209-61] (ab284387)) and RUNX2 ([EPR22858-106] (ab236639)) were purchased from Abcam (Cambridge, MA, USA). Rabbit monoclonal antibodies against smad1/5/9 and phosphorylated (p)-smad1/5/9 were kindly provided by Dr. Cao (Guangzhou, China). Tissue ALP activity assay kit and Naringin were purchased from Solarbio Science & Technology Co., Ltd. (Beijing, China). Thermolysin was obtained from Bacillus thermoproteolyticus by Sigma-Aldrich Inc. (St. Louis, MO, USA). ER $\alpha$  Recombinant Protein was purchased from Thermo Fisher Scientific Inc (Waltham, MA, USA).

### 2.2. RDNVs isolation and purification

As shown in Fig. 1, fresh Rhizoma Drynariae and phosphate-buffered saline (PBS) solution (1:2.5, g/mL) were placed in a blender and chopped at a high speed for 10 min. The obtained juices were centrifuged at 500  $\times$ g for 20 min, 2000  $\times$ g for 30 min, and 10,000  $\times$ g for 60 min at 4 °C (Baiyang, R18, Beijing, China) to remove the large plant tissues and cell debris. Subsequently, RDNVs were collected by ultracentrifugation at 100,000  $\times$ g for 70 min and re-suspended in PBS. RDNVs were filtered using a 0.22  $\mu$ m filter and washed once more with PBS. The protein concentration of the samples was determined using the BCA protein assay kit following the manufacturer's instructions. The resultant RDNVs were stored at -80 °C until further use.

### 2.3. Physical characterization of RDNVs

The morphology of RDNVs was observed and photographed under a transmission electron microscope (TEM) (JEM-1200EX, JEOL Ltd., Japan). RDNVs were assayed with a Flow NanoAnalyzer (nanoFCM) (Xiamen Fuli Biotechnology Co., Fujian, China), a technique for determining small particle size

distribution profiles in suspensions using known standards. A 250 nm quality control particle calibration laser was used as a reference for particle concentration. A mixture of particles of different sizes (68–155 nm) was used to generate the reference curve of the diameter distribution. The sample particle concentration and size distribution were calculated using NF Profession 1.0 (Xiamen Fuli Biotechnology Co., China).

The Triton X-100 membrane rupture test indirectly indicates the purity of RDNVs. The RDNVs were equally divided into six test tubes, to which 0, 0.01%, 0.025%, 0.05%, 0.1%, or 0.5% (volume ratio to PBS) Triton X-100 was added and mixed vigorously for 30 s. The mixture was incubated for 30 min at room temperature and the number of particles of RDNVs was determined using a Flow NanoAnalyzer.

### 2.4. RNA, protein, and lipid characterization of RDNVs

To determine whether RDNVs contain RNAs, RDNVs with and without RNase A (Solarbio, Beijing, China) were incubated for 30 min at 37 °C. RNAs were extracted with the RNeasy Mini Kit (QIAGEN, Hilden, Germany) and detected by 3% agarose gel electrophoresis.

RDNVs were lysed by adding an exosome-specific lysing solution. A 10% sodium dodecyl sulfate-polyacrylamide gel electrophoresis (SDS-PAGE) gel was prepared according to the PAGE Gel Rapid Prep Kit (10%) (Epizyme Biotech, Shanghai, China). RDNV proteins (20  $\mu$ g) were added in each gel well, and the gel after electrophoresis was stained according to the instructions of the Coomassie brilliant blue staining kit (Biosharp) and imaged using a chemiluminescence imaging system (Clix Science Instruments Co., Ltd., Shanghai, China).

To purify lipids from RDNVs, RDNVs were mixed with chloroform and methanol in a ratio of 3:8:4 (v/v/v) and centrifuged at 10,000  $\times$ g for 10 min, after which the sample was divided into three layers (the upper water, middle protein, and bottom lipid layers). The bottom layer was collected and dried at 100 °C. Subsequently, it was resuspended with chloroform, and the lipids were detected by thin-layer liquid chromatography (TLC).

### 2.5. Experimental animals

Female C57BL/6J mice aged 8 weeks were purchased from RuiYe Laboratory Animal Corporation (Guangdong, China) and the Animal Experiment Center of Guangzhou University of Traditional Chinese Medicine (Guangdong, China) and maintained in specific pathogen-free cages with standard food and water. Humane care was provided to each animal during the experiments according to the criteria outlined in the Guide for the Care and Use of Laboratory Animals published by the National Institutes of Health (NIH) (National Research Council 2011). All experimental procedures were executed according to the protocols approved by the Guangzhou University of Chinese Medicine Animal Care and Use Committee (20201201001).

### 2.6. In vivo imaging experiments

To track the *in vivo* biodistribution of RDNVs after intravenous injection (i.v.) or intraperitoneal administration (i.p.), a near-infrared fluorescence probe (DiR) was used to label RDNVs. DiR solution (10  $\mu$ mol/L) was added to an RDNVs suspension of  $1 \times 10^{11}$  particles and incubated for 30 min at 37 °C in the dark. Finally, the free DiR was removed by ultracentrifugation at

100,000  $\times g$  for 70 min at 4 °C, the precipitate was washed three times with PBS, and the purified DiI-labeled RDNVs were obtained. DiI-labeled RDNVs were administered to C57BL/6J mice at an equivalent DiI concentration ( $5 \times 10^{11}$  particles/kg body weight) via an i.v. or i.p. route. The mice were euthanized at 6, 24, 48, or 72 h after administration to obtain the femurs and main organs (heart, liver, spleen, lung, and kidney). Images were captured using an IVIS spectrum imaging system Lumina III (PerkinElmer, MA, USA). PBS or free DiI application was considered as a control in this study.

### 2.7. *In vivo cellular uptake profiles of RDNVs*

Female C57BL/6J mice aged 8 weeks were euthanized by neck dislocation after i.v. administration of DiI-labeled RDNVs ( $5 \times 10^{11}$  particles/kg body weight) for 12, 24, 48, or 72 h. The surrounding tissues were removed rapidly, the femur and tibia were separated, and bone-biting forceps were used to remove the epiphysis. PBS was used to repeatedly wash out the medullary cavity until the osseous substance appeared slightly bright. The washing fluid of the medullary cavity was collected and simultaneously labeled with scoa-1-FITC, a positive marker on the surface of mouse bone marrow mesenchymal stem cells for FCM.

### 2.8. *Osteoporosis animal model and in vivo anti-osteoporosis experiments*

Female C57BL/6J mice aged 8 weeks were anesthetized with 10% pentobarbital by i.p. administration. The mice were then randomly assigned to the following groups ( $n = 3$  in each group): sham-operated (Sham), and ovariectomized (OVX). After 12 weeks, the mice were treated with RDNVs of  $1 \times 10^9$  (low concentration) and  $2 \times 10^9$  (high concentration) particles/ $\mu\text{L}$  (volume 100  $\mu\text{L}$ ) via i.p. administration every other day for 3 weeks after the Sham and OVX operation. Mice of the control and Sham group were given the same dose of PBS as a placebo. Following RDNVs treatment, the mice were euthanized by cervical dislocation, and the femurs were collected for further analysis, including micro-computed tomography (micro-CT) imaging, determining bone-related indexes and hematoxylin-eosin staining. Tissues (liver, spleen, kidneys, femur) and eye blood were collected for evaluation of RDNVs biocompatibility. The levels of serum Ca and liver function-related parameters (serum alanine transaminase (ALT), total protein (TP)) and kidney function-related parameters [blood urea nitrogen (BUN) and serum creatinine (Crea)] from control and RDNVs-treated mice were detected by Automatic Biochemical Analyser (AU5800, Beckman Coulter, CA, USA). ALP in femoral tissue was detected by Enzyme-linked immunosorbent assay (ELISA).

### 2.9. *Micro-CT analysis*

Three months after OVX surgery, mouse femurs were collected, fixed in 4% PFA for 48 h at 4 °C, and scanned with a Scanco mCT 50 (Scanco Medical, Zurich, Switzerland) set to a voltage of 70 kV and a resolution of 10  $\mu\text{m}$ . For the femurs, 100 slices below the femur growth plate were measured for three-dimensional reconstruction and trabecular bone quantification, and 30 slices of the cortex bone area in the middle of the femur were reconstructed for statistical analysis. To examine the trabecular structures of the femurs, the following six parameters were calculated: bone mineral density (BMD,  $\text{g}/\text{mm}^3$ ), bone volume (BV,  $\text{mm}^3$ ), bone

volume ratio (BV/TV, %), trabecular number (Tb. N, 1/mm), trabecular pattern factor (Tb. Pf, 1/mm), and structure model index (SMI, 1).

### 2.10. *The hBMSC identification and culture*

The hBMSCs were laboratory-frozen cell lines (BluefBio, Shanghai, China). CD34-fluorescein isothiocyanate (FITC), CD44-FITC, CD73-FITC, and CD105-FITC mouse anti-human monoclonal antibodies as well as isotype antibody IgG1 (2  $\mu\text{L}$  each test), respectively, were added in cell suspension ( $3 \times 10^5$  cells in 100  $\mu\text{L}$ ). The mixture was first incubated for 30 min at room temperature followed by 30 min in the dark after adding the secondary antibody. Flow cytometry (FCM) (BriCyte E6; Mindray Biotechnology Co., Guangdong, China) was adopted to identify the expression of specific surface markers of hBMSCs.

### 2.11. *Osteogenic differentiation and alizarin red staining (ARS) staining of hBMSCs*

To confirm the pro-osteogenic property of RDNVs, the osteogenic differentiation assay for hBMSCs was performed. In brief, hBMSCs were seeded in six-well plates at a  $1 \times 10^5$  cell density per well. The osteogenic-inducing complete medium (CM) consisted of Dulbecco's modified Eagle's media (DMEM) containing Nutrient Mixture F-12, 10% fetal bovine serum (FBS), 1% penicillin–streptomycin mixed solution, 0.1  $\mu\text{mol}/\text{L}$  dexamethasone, 10  $\text{mmol}/\text{L}$   $\beta$ -glycerophosphate and 50  $\mu\text{g}/\text{mL}$  ascorbic acid. hBMSCs were exposed to RDNVs suspensions (20  $\mu\text{g}/\text{mL}$  in 2 mL) with or without 1  $\mu\text{mol}/\text{L}$  ICI 182,780 for 14 days. As a positive control, hBMSCs were exposed to osteogenic-inducing CM with or without 1  $\mu\text{mol}/\text{L}$  ICI 182,780 for 14 days. Half the volume of the CM of all groups was changed every 3 days thereafter. Cells were collected for ARS, quantitative reverse transcription-polymerase chain reaction (qRT-PCR), and Western blotting on Days 7 and 14 of osteogenic differentiation induction.

### 2.12. *Cell viability assay*

The hBMSCs were grown in 96-well plates at a final density of  $1 \times 10^3$  cells per well and incubated overnight. Subsequently, the CM was exchanged to a serum-free medium containing RDNVs (protein concentration: 20  $\mu\text{g}/\text{mL}$ ) and co-incubated for 24, 48, or 72 h. Following incubation, the cells were rinsed with PBS to remove excess RDNVs, CCK-8 reagent was added, and the cells were incubated at 37 °C for 2 h. Finally, the absorbance was measured at 450 nm using a microplate reader (RaytoRT-2100C; Rayto Life and Analytical Sciences Co., Ltd., Shenzhen, China) to determine cell viability.

### 2.13. *In vitro cellular uptake profiles of RDNVs*

To quantitatively and qualitatively study the cellular uptake profiles of RDNVs, an orange-red fluorescence probe (DiI) was used to label these NVs. DiI solution (10  $\mu\text{mol}/\text{L}$ ) was added to RDNVs suspension of  $1 \times 10^{11}$  particles and this mixture was incubated for 30 min at 37 °C in the dark. Free DiI was removed by ultracentrifugation at 100,000  $\times g$  for 70 min at 4 °C, and the precipitate was washed three times with PBS. Finally, purified DiI-labeled RDNVs were obtained, and protein concentration was determined by a BCA kit.

The hBMSCs were seeded in 6-well plates at a density of  $1 \times 10^5$  cells per well and incubated overnight. Subsequently, the complete culture medium was exchanged with serum-free medium containing DiI-labeled RDNVs (protein concentration: 10 and 20  $\mu\text{g}/\text{mL}$ ). Following co-incubation for 6, 12, 24, and 48 h at 37 °C, the cells were washed three times with PBS to remove the excess NVs and re-suspended in PBS for FCM analysis. Or hBMSCs were fixed with paraformaldehyde solution (PFA, 4%, v/v) for 10 min. Hoechst33343 was used to stain the nucleus. Finally, fluorescent images of the cells were acquired using a fluorescence microscope (Leica, Wetzlar, Germany).

To determine the effects of temperature on RDNVs internalization, hBMSCs were incubated with 20  $\mu\text{g}/\text{mL}$  of DiI-RDNVs for 24 h at 37, 22 and 4 °C, after washing with 3 times PBS, cells were fixed with 4% PFA for 15 min. Finally, cells were coverslip-mounted with Hoechst33343 and FITC-Phalloidin for fluorescence imaging.

To investigate the possible internalization mechanism, special inhibitors [indomethacin (100  $\mu\text{mol}/\text{L}$ ), chlorpromazine (25  $\mu\text{mol}/\text{L}$ ), amiloride (250  $\mu\text{mol}/\text{L}$ ), and cytochalasin D (10  $\mu\text{mol}/\text{L}$ )] were first incubated with hBMSCs for 1 h at 37 °C, then 20  $\mu\text{g}/\text{mL}$  of DiI labeled RDNVs were added for additional 48 h incubation. After washing with 3 times PBS, cells were fixed with 4% PFA for 15 min. Finally, cells were coverslip-mounted with Hoechst33343 and FITC-Phalloidin for fluorescence imaging.

#### 2.14. RNA isolation, reverse transcription, and real-time PCR

Total RNA was isolated using TRIzol reagent according to the manufacturer's instructions and quantified by determining the absorbance at 260 nm. The total RNA (1  $\mu\text{g}$ ) was incubated with 5  $\times$  Primescript RT Master Mix 2  $\mu\text{L}$  (Takara Standard Co. Ltd., Osaka, Japan) at 85 °C for 5 s and cooled immediately on ice. The cDNA was amplified in a reaction mixture containing SYBR Green PCR Master Mix (Covin bio, Taizhou, China) and 1 mmol/L gene-specific primer using a PCR kit (QIAGEN). The amplification protocol consisted of an initial step of 95 °C for 5 min followed by 40 cycles of 95 °C for 10 s, 60 °C for 15 s and 72 °C for 20 s. Fold changes of mRNA were calculated by the  $2^{-\Delta\Delta\text{Ct}}$  method after normalization to the GAPDH expression. Supporting Information Table S1 shows the list of the qPCR primers used.

#### 2.15. Western blot analysis

The hBMSCs were lysed in RIPA Lysis buffer (Beyotime, Shanghai, China) containing 1% protease inhibitor cocktail (Sigma-Aldrich, St. Louis, MO, USA), 1 mmol/L phenylmethylsulfonyl fluoride (Sigma-Aldrich) and 1 mmol/L phosphatase inhibitor (Sigma-Aldrich) for 30 min. Protein concentrations were assessed using a BCA protein assay reagent. Subsequently, 20 mg total protein was separated by SDS-PAGE on a 10% gel and transferred electrophoretically to a nitrocellulose filter membrane (HATF00010, Millipore, Billerica, MA, USA). BMP2, ER $\alpha$ , and GAPDH antibodies were used at a dilution of 1:1000. The RUNX2 antibody was purchased from Boster (Shanghai, China) and used at a dilution of 1:500.

#### 2.16. Metabolomics and bioinformatics analysis

The effective biological components of RDNVs were further investigated through metabolomics and bioinformatics analysis.

Lyophilized RDNVs were mixed with 400  $\mu\text{L}$  methanol, and 100  $\mu\text{L}$  processed RDNV sample was aspirated with a syringe. The non-targeted metabolomics data of the RDNVs samples were detected using a liquid mass spectrometry system consisting of a high-performance liquid chromatograph (Thermo Fisher Scientific Dionex U3000 UHPLC, Waltham, MA, USA) and a tandem high-resolution mass spectrometer (Thermo Fisher Scientific QE, Waltham, MA, USA).

The active ingredients of RDNVs were retrieved from the Chinese medicine comprehensive database (TCMID, <http://119.3.41.228:8000/tcmid/>), the Chinese medicine systematic pharmacology database and analysis platform (TCMSP, <https://tcmssp.com/tcmssp.php>), and the Chinese medicine evidence association database (SymMap, <https://www.symmap.org>). The metabolomic components of the obtained RDNVs were intersected with those of *Rhizoma Drynariae* to obtain common components between them.

#### 2.17. Surface plasmon resonance (SPR)

To-be-tested substances were assayed by ER $\alpha$  protein binding assay (SPR method) in collaboration with Shanghai Medicilon Inc. Briefly, different concentrations of positive control Estradiol or experimental drug Naringin were bound 1:1 to 50  $\mu\text{g}/\text{mL}$  ESR1 (ER $\alpha$ ) pH 4.5 using an instrument Biacore 8K (GE Healthcare). CM5 microarray activation: 400 mmol/L EDC and 100 mmol/L NHS 10  $\mu\text{L}/\text{min}$  flow rate for 600 s; microarray coupling: the target protein was activated for 600 s; microarray coupling: the target protein was activated for 600 s by 400 mmol/L EDC and 100 mmol/L NHS 10  $\mu\text{L}/\text{min}$  flow rate. Activation: 400 mmol/L EDC and 100 mmol/L NHS at a flow rate of 10  $\mu\text{L}/\text{min}$  for 600 s. Microarray coupling: target protein ER alpha was diluted to 50  $\mu\text{g}/\text{mL}$  with 10 mM sodium acetate (pH 4.5) at a flow rate of 5  $\mu\text{L}/\text{min}$  for 2000 s. Microarray closure: 1 mol/L ethanolamine was closed at a flow rate of 10  $\mu\text{L}/\text{min}$  for 600 s. Input analysis: The sample was analyzed by 4-fold dilution of the target protein starting from 500  $\mu\text{mol}/\text{L}$  in PBS (pH 7.4), and a total of 7 tests were performed at a flow rate of 10  $\mu\text{L}/\text{min}$  for 180 s for binding and 180 s for dissociation.

#### 2.18. High-performance liquid chromatography (HPLC)

RDNVs (10 mL,  $1 \times 10^{11}$  particles/mL) were evaporated to dryness at 100 °C, dissolved in methanol, and transferred to a flask. Following refluxing, sonication, and filtration, the mixture was evaporated to 1 mL in a 100 °C water bath. The mobile phases were acetic acid and methanol, and the wavelength was 283 nm. There were three standard ingredients naringin, narirutin, and naringenin. The naringin standard was tested with five concentration gradients (60, 30, 15, 7.5, and 3.75  $\mu\text{g}/\text{mL}$ ) and a standard curve was generated (Supporting Information Fig. S1).

#### 2.19. Drug affinity responsive target stability (DARTS)

Make a starting stock concentration of 50 mmol/L compounds, dilute the compound to 25 mmol/L with  $1 \times$  TNC ( $10 \times$  TNC: 500 mmol/L Tris-HCl (pH8.0), 500 mmol/L NaCl, 100 mmol/L CaCl<sub>2</sub>). Add either 0.8  $\mu\text{L}$  of 25 mmol/L Naringin to 40  $\mu\text{L}$  ER $\alpha$  Recombinant Protein, and 0.8  $\mu\text{L}$  50% DMSO was added to the vehicle group ( $1 \times$  TNC). Incubate ER $\alpha$  with the solutions for 60 min at room temperature. On the ice, establish serial dilutions (Thermolysin: ER $\alpha$  protein ratios: 1:10, 1:50, 1:250) of freshly

thawed Thermolysin solution in  $2 \times$  TNC. Add 10  $\mu$ L of the range of Thermolysin solutions in each sample. After 60 min, halt digestion *via* the addition of 5  $\mu$ L of 0.5 mol/L EDTA. Dilute samples with the appropriate volume of NuPAGE™ LDS Sample Buffer and boil at 95 °C for 5 min. Next, the samples were subjected to SDS-PAGE analyses.

### 2.20. Statistical analysis

The data are expressed as the mean  $\pm$  SEM. Significance between experimental groups was determined by independent sample *t*-tests or chi-square tests (only for the comparisons of positive cell ratios) using SPSS 24.0. Values of  $*P < 0.05$  (two-tailed) were statistically significant. Bar charts were produced using GraphPad Prism 9 software.

## 3. Results

### 3.1. Physicochemical characterization of RDNVs

RDNVs were obtained and purified from fresh Rhizoma Drynariae by differential centrifugation (Fig. 1). Transmission electron microscope (TEM) showed a typical cup-shaped vesicle structure and an intact cell membrane structure (Fig. 2A). Flow NanoAnalyzer revealed that the RDNVs had a mean particle size

distribution of  $75.7 \pm 15.8$  nm (Fig. 2B). Therefore, the mean particle sizes of RDNVs determined by TEM and Flow NanoAnalyzer were consistent. The yield of RDNVs extracted from 1 kg fresh Rhizoma Drynariae was approximately 20 mg. Its purity was approximately  $4.17 \times 10^{11}$  particles/mg. Based on membrane structure, we performed membrane solubilization using Triton X-100, a surfactant that disrupts membrane integrity. The particle concentration of RDNVs gradually decreased with increasing Triton X-100 concentration, and compared with an absence of Triton X-100, the number of particles when treated with 0.5% Triton X-100 decreased significantly to 28% (Fig. 2C). Nanoview examination showed an electric potential of  $-43.2 \pm 0.04$  mV (Fig. 2D).

To investigate the stability of RDNVs *in vitro*, three batches of RDNVs were subjected to different pH conditions to simulate the intragastric (pH = 1.2) and intestinal (pH = 6.5) environment and the results show that particle size and concentration were stable (Supporting Information Fig. S2). Therefore, we could isolate stable, reliable, and abundant RDNVs from the natural traditional Chinese medicine Rhizoma Drynariae.

Cell-derived NVs are present in most body fluids containing proteins, RNAs, and lipids<sup>32</sup>. We investigated the RNAs, proteins, and lipids of RDNVs by agarose gel electrophoresis, polyacrylamide gel electrophoresis, and TLC, respectively. We found that RDNVs contained small-molecular-weight (15–35 kDa) proteins, large molecular weight RNAs sensitive to degradation by

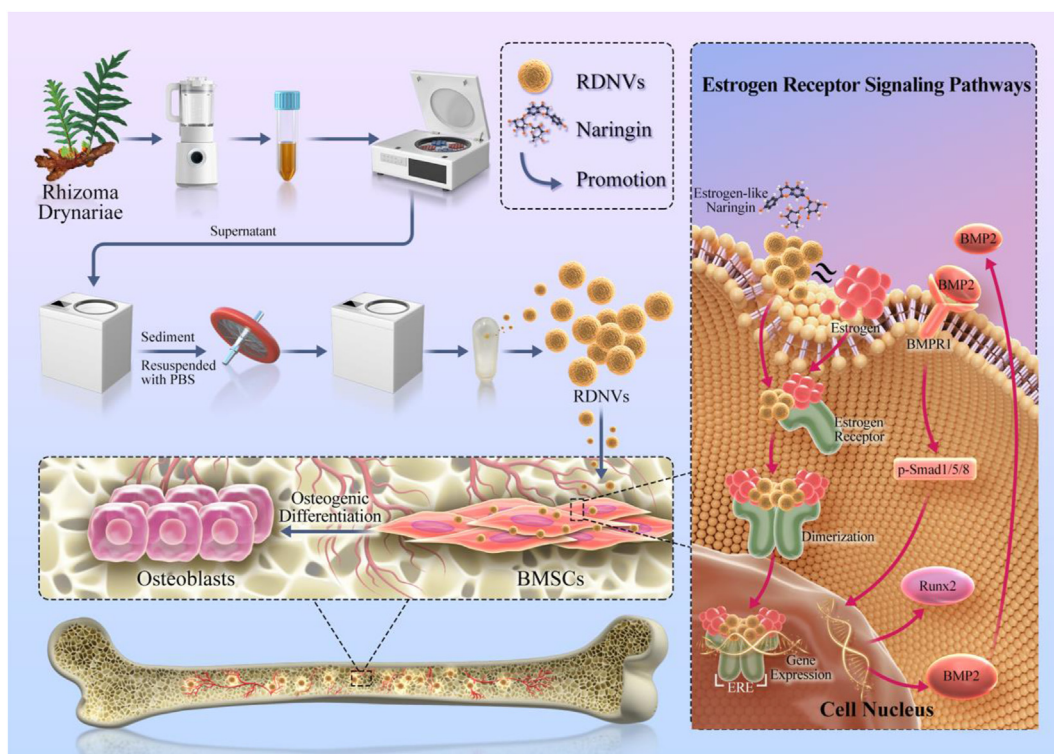


**Figure 1** Schematic illustration of RDNVs reverse osteoporosis by potentiating osteogenic differentiation of hBMSCs *via* targeting estrogen receptor  $\alpha$  (ER $\alpha$ ) signaling. RDNVs, a natural product isolated from fresh Rhizoma Drynariae root juice by differential ultracentrifugation, exhibited potent bone tissue-targeting activity and anti-osteoporosis efficacy in an ovariectomized mouse model. RDNVs, effectively internalized by hBMSCs, enhanced proliferation and ER $\alpha$  expression levels of hBMSC, and promoted osteogenic differentiation and bone formation. Mechanistically, *via* the ER $\alpha$  signaling pathway, RDNVs facilitated mRNA and protein expression of bone morphogenetic protein 2 and runt-related transcription factor 2 in hBMSCs, which are involved in regulating osteogenic differentiation. Further analysis revealed that naringin, existing in RDNVs, was the active component targeting ER $\alpha$  in the osteogenic effect.

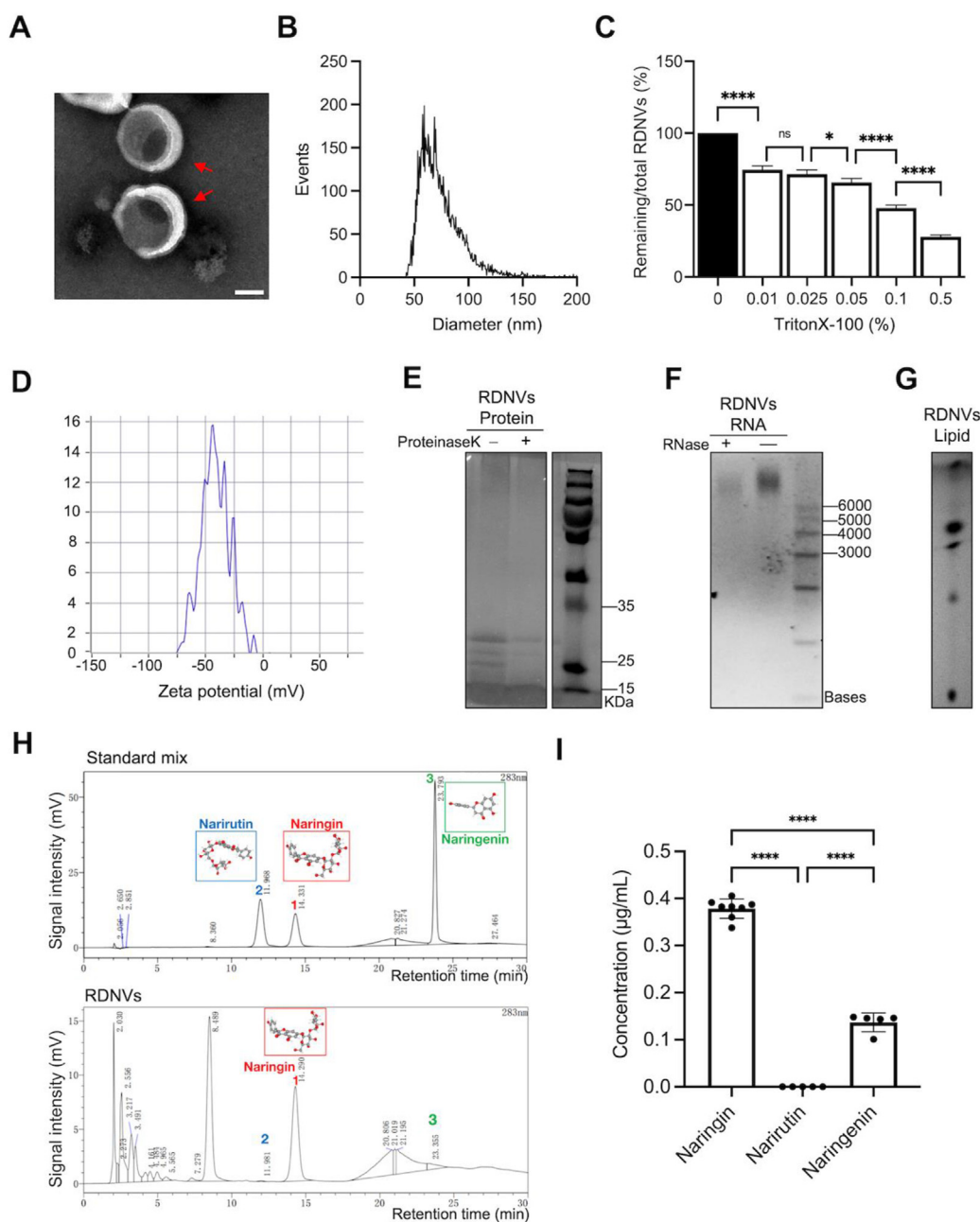


**Figure 2** Identification and physicochemical characterization of RDNVs. (A) The morphology of RDNVs determined by TEM (scale bar = 50 nm). (B) The particle size distribution of RDNVs was detected by Flow NanoAnalyzer. (C) RDNVs were incubated with TritonX-100 and its Purity is indirectly demonstrated by membrane rupture efficiency. Data are presented as mean  $\pm$  SD ( $n = 3$ ),  $*P < 0.05$ ,  $****P < 0.0001$ . ns, no significance. (D) Surface charge of RDNVs determined by Nanoview. The main components in RDNVs: (E) proteins incubated with or without ProteinaseK determined by SDS-PAGE, (F) RNAs incubated with or without RNase determined by agarose gel electrophoresis and (G) total lipids determined by TLC. (H) The standard ingredients naringin, narirutin and naringenin and their contents in RDNVs were determined by HPLC. Chromatographic column: Megres C18 (4.6 mm  $\times$  150 mm, 5  $\mu$ m). (I) Comparison of the concentration of the three active ingredients (Naringin, Narirutin, Naringenin) in RDNVs. Data are presented as mean  $\pm$  SD ( $n = 5$ ),  $****P < 0.0001$ .

ribonuclease and different forms of lipids (Fig. 2E–G), indicating that RDNVs may play a role in intercellular signaling as well as a wide range of biological functions through the proteins, RNAs, and lipids.

The traditional Chinese medicine characteristic map technology is applied to evaluate the quality of medicinal materials with good stability and accuracy. To determine whether the obtained

RDNVs shared the characteristic map with Rhizoma Drynariae, we obtained High-Performance Liquid Chromatography (HPLC) profiles according to the national drug standard of “Gusuibu Peifangkeli” issued by the State Drug Administration. There were four characteristic peaks in the chromatogram of the RDNVs sample, which corresponded to those in the reference substance of Rhizoma Drynariae (Supporting Information Fig. S3A). The

peak corresponding to the naringin reference substance is the S peak or peak 4, which was found to be present in RDNVs (Fig. S3B–S3D). The relative retention time was within  $\pm 10\%$  of the specified value: 0.40 (peak 1), 0.41 (peak 2), and 0.89 (peak 3). Specified values were: 0.44 (peak 1), 0.45 (peak 2), and 0.89 (peak 3). The characteristic profiles of RDNVs were stable from batch to batch.

To determine the main components of RDNVs, we further quantified naringin, naringin, and naringenin by comparing them against the standards of the three flavonoids by HPLC. The results showed that naringin existed in RDNVs with a concentration of approximately 0.3  $\mu\text{g}/\text{mL}$  ( $n = 5$ ), whereas there was very little naringin and naringenin in RDNVs. The concentration of naringin in different batches of RDNVs was stable (Fig. 2H and I). Overall, these results indicated that naringin, which existed in RDNVs, is involved in these NVs exerting their promising effects on targeting the bone and the treatment of PMOP.

### 3.2. RDNVs are bone-targeted *in vivo*

Both intravenous (i.v.) injection and intraperitoneal (i.p.) administration are common modes of administration. To determine the distribution of RDNVs *in vivo*, DiR-labeled RDNVs ( $5 \times 10^{11}$  particles/kg body weight) were administered to female C57BL/6J mice. As presented in Supporting Information Fig. S4, RDNVs were gradually accumulated in the femur for 48 h by i.v. injection. The maximum enrichment amount of RDNVs in the femur was found at the time point of 48 h after both i.v. injection (Fig. 3A and C) and i.p. administration (Fig. 3B and D). Moreover, the maximum fluorescence intensity of the femur in the RDNVs (i.v.)-treated group was much stronger than that in the RDNV (i.p.)-treated group (Fig. 3C and D). Subsequently, the distribution profiles of RDNVs in the five major organs (heart, liver, spleen, lung, and kidney) at different time points (12, 24, 48, and 72 h) were investigated. Significant quantities of RDNVs were observed in the liver following i.v. injection and i.p. administration, with a lesser presence in the spleen and lung. Additionally, the fluorescence signals of RDNVs in these three organs exhibited a slight decline within 24 h post-administration (Fig. 3C and D). Furthermore, to identify the beneficial role of RDNVs in i.v. and i.p. delivery of their components, the *in vivo* distribution profile of free DiR fluorescence dye was also investigated. As shown in Fig. 3A, some DiR dye was detected in the liver, spleen, and lung after i.v. administration, but no free DiR dye was distributed in the femur, in comparison with the mouse group that received i.v. DiR-labeled RDNVs. Consistent with this, some DiR dye was distributed in the liver and spleen and minimal DiR was in the lung and kidney after i.p. administration, but no free DiR dye was detected in the femur, in comparison with the mouse group that received i.p. DiR-labeled RDNVs (Fig. 3B). These observations implied that i.p. administered RDNVs were maintained stably in the mouse body, entered the circulatory system, and accumulated in the femur sites.

To further verify the targeting properties of RDNVs to bone tissues, we isolated mouse bone marrow mesenchymal stem cells (mBMSCs) of the femur from female C57BL/6J mice after i.v. and i.p. injection of DiI-labeled RDNVs at different time points (48 and 72 h), and the efficiency of DiI-labeled RDNVs labeling of mBMSCs was determined. Fig. 3E and F show that the positive rate of DiI-labeled RDNVs uptake by mBMSCs *in vivo* could reach  $>35\%$  at 48 h. Overall, these results indicated that on RDNVs treatment, RDNVs were taken up *in vivo* by BMSCs in the femur.

### 3.3. RDNVs mitigate bone loss *in vivo*

To evaluate the therapeutic effects of RDNVs against PMOP, an ovariectomized (OVX) mouse model was established. Intraperitoneal (i.p.) injection prevents NVs from entering the circulation directly greatly reduces the clearance of the liver and spleen<sup>33</sup>, and is much more secure and operable than i.v. injection. Mouse was treated with RDNVs once every 2 days at a dose of  $1 \times 10^{11}$  (low concentration) or  $5 \times 10^{11}$  (high concentration) particles/kg body weight *via* i.p. injection for 3 weeks (Fig. 4A). Serum calcium and femoral alkaline phosphatase (ALP) activity were measured in mice, and the results showed that RDNVs reversed the bone calcium deficiency and femoral ALP elevation caused by osteoporosis (Fig. 4B). Right femurs were obtained and subjected to micro-CT analysis of the trabecular architecture. As shown in Fig. 4C, compared to Sham (control) mice, the trabecular structure of distal femurs in OVX mice was severely impaired. In quantitative analyses, the bone mineral density (BMD), bone volume (BV), BV/TV, and trabecular number (Tb. N) were largely reduced, whereas the trabecular pattern factor (Tb. Pf) and structure model index (SMI) were increased in OVX mice compared to sham mice (Fig. 4D), indicating that the success of our OVX model in terms of bone loss. Importantly, RDNVs at the high dosage concentration ( $2 \times 10^9$  particles) reversed the ovariectomy-induced disorder of the trabecular architecture (Fig. 4C). RDNVs treatment suppressed the ovariectomy-induced reduction of the BMD, BV, BV/TV, and Tb. N and inhibited the ovariectomy-induced increase of the Tb. Pf and SMI (Fig. 4D). Taken together, these results demonstrated that RDNVs could effectively alleviate bone loss *in vivo* to prevent or reverse osteoporosis.

To evaluate the pharmaco-toxicological characteristics of RDNVs, we subsequently analyzed *in vivo* RDNVs biocompatibility *via* i.p. administration of RDNVs or PBS into mice once every 2 days for 3 weeks. Strikingly, we found no apparent signs of tissue impairments in the major organs (liver, spleen, kidney, or femur) and serological abnormality in liver or kidney function-related parameters from two mouse groups (Fig. 4E and F). Compared with the risk for nephrotoxicity in long-term *Rhizoma Drynariae* use in clinical treatment, repeated RDNVs administration *via* the i.p. route appeared relatively safe for organisms. Collectively, RDNVs extracted from fresh *Rhizoma Drynariae* could be considered natural drug-loaded NVs and have a promising potential in PMOP treatment without loading additional drugs.

### 3.4. RDNVs could be taken up by hBMSCs *in vitro*

Bone marrow mesenchymal stem cells (BMSCs) have strong osteogenic differentiation potential and are excellent seed cells for bone tissue engineering<sup>34</sup>. The active components of the natural NVs exert their biological functions mainly within cells, thus their cellular uptake by hBMSCs is essential.

To verify the successfully obtained primary hBMSCs, we first performed marker identification on the collected cells. Specific surface markers of hBMSCs, including being negative for CD34 and positive for CD29, CD73, and CD105, were identified *via* flow cytometry to confirm that the cells collected were hBMSCs (Fig. 5A). To demonstrate that RDNVs can be taken up and absorbed by hBMSCs, RDNVs were labeled using the lipophilic fluorescent dye DiI. DiI-labeled RDNVs (orange-red fluorescence)

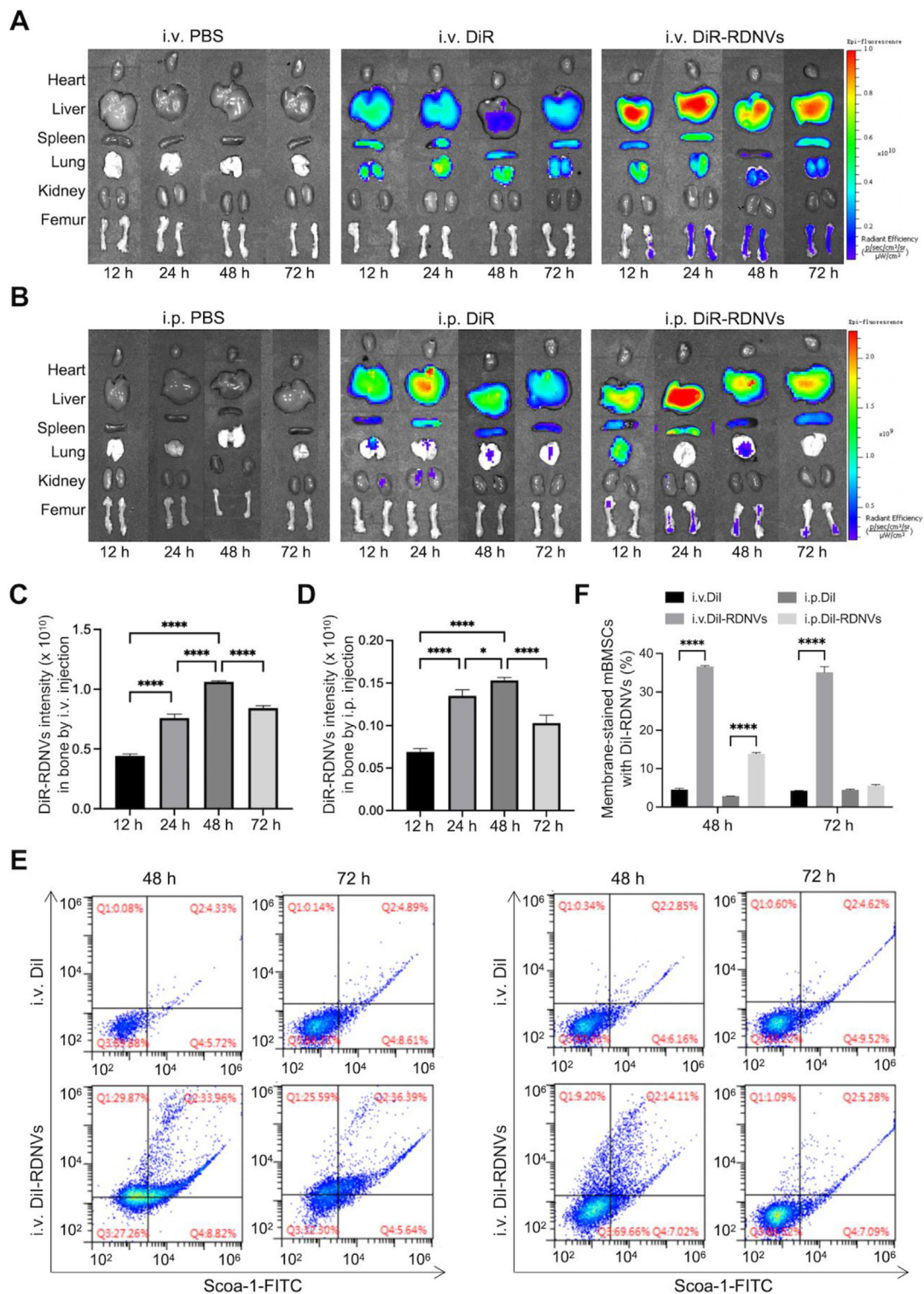


**Figure 3** Bio-distribution of RDNVs *in vivo*. (A) Fluorescence imaging and (C) fluorescence quantification in the heart, liver, spleen, lung, kidney and femur after i.v. administration of PBS, DiR and DiR-labeled RDNVs in mice at different time points (12, 24, 48, and 72 h). (B) Fluorescence imaging and (D) fluorescence quantification in the heart, liver, spleen, lung, kidney, and femur after i.p. administration of PBS, DiR and DiR-labeled RDNVs in mice at different time points (12, 24, 48, and 72 h). (E, F) mBMSCs cellular uptake profiles *in vivo* were detected by FCM analysis after i.v. and i.p. administration of DiI and DiI-labeled RDNVs ( $5 \times 10^{11}$  particles/kg body weight) in mice at 12, 24, 48, and 72 h. Data are presented as mean  $\pm$  SD ( $n = 3$ ). \*\*\*\* $P < 0.0001$ .

were internalized by hBMSCs, and these NVs were mainly distributed in the cytoplasm around the nucleus (Fig. 5B). The cellular uptake of DiI-labeled RDNVs by hBMSCs increased in a time-dependent manner (Fig. 5C and D). Following co-incubation for 48 h, the cell internalization percentage of DiI-labeled RDNVs by hBMSCs reached >90%. In addition, there was a concentration-dependent effect of DiI-labeled RDNVs, whereby the cell internalization percentages of 20  $\mu\text{g}/\text{mL}$  RDNVs were higher than those of 10  $\mu\text{g}/\text{mL}$  RDNVs at all the time points. These results suggested that 20  $\mu\text{g}/\text{mL}$  RDNVs were more effectively internalized by hBMSCs at 48 h.

To discover the effect of temperature on RDNVs internalization, DiI-RDNVs (20  $\mu\text{g}/\text{mL}$ ) were incubated with hBMSCs for 48 h under different temperatures (4  $^{\circ}\text{C}$ , 22 and 37  $^{\circ}\text{C}$ ), and cell internalization is influenced by temperature (Fig. 5E), with the optimum internalization temperature being 37  $^{\circ}\text{C}$ .

To investigate the potential endocytosis mechanism of RDNVs, DiI-RDNVs (20  $\mu\text{g}/\text{mL}$ ) were added for incubate 48 h after four endocytosis inhibitors (Indomethacin, amiloride, cytochalasin D, and chlorpromazine) were incubated for 1 h with hBMSCs<sup>35</sup>. Four endocytosis inhibitors could significantly inhibit the internalization of RDNVs (Fig. 5F), indicating caveolae-mediated endocytosis involved in RDNVs' cellular uptake.

### 3.5. Pro-proliferative and pro-differentiation activities of RDNVs to hBMSCs in vitro

Considering that RDNVs contained a considerable amount of anti-PMOP metabolites, their pro-proliferative activities on hBMSCs were evaluated using the CCK-8 assay. RDNVs displayed clear pro-proliferative capacities for hBMSCs after co-incubation at 24 and 48 h (Fig. 6A). Moreover, we found that RDNVs exerted the most significant promotional effect on hBMSCs at an intermediate protein concentration (20  $\mu\text{g}/\text{mL}$ ) but not at 10  $\mu\text{g}/\text{mL}$ , which could be interpreted as these natural NVs displaying pro-proliferative activities at a moderate reaction time and protein concentrations (20  $\mu\text{g}/\text{mL}$ ). To verify the biosafety of RDNVs against hBMSCs, an apoptosis assay was conducted (Fig. 6B). There was no significant difference in the apoptosis rate at any of the time points between any of the different concentrations (10 and 20  $\mu\text{g}/\text{mL}$ ) of RDNVs, indicating that they had no effects on hBMSCs to inhibit their apoptosis.

Because the flavonoid structure is similar to that of estrogen and Rhizoma Drynariae has phytoestrogen-like effects<sup>36</sup>, we hypothesized that RDNVs isolated from fresh Rhizoma Drynariae acted as an ER $\alpha$  agonist to activate the estrogen pathway. To further characterize RDNVs as an ER $\alpha$  modulator, we investigated whether RDNVs directly upregulated ER $\alpha$  mRNA. We found that RDNVs time-dependently enhanced ER $\alpha$  mRNA expression levels during hBMSC proliferation (Fig. 6C). After 48 h intervention with hBMSCs at 20  $\mu\text{g}/\text{mL}$  RDNVs, the relative expression levels of ER $\alpha$  mRNA in hBMSCs increased significantly. However, whether RDNVs promoted hBMSC osteogenic differentiation and its mechanism need to be further investigated.

Considering that RDNVs acted as an ER $\alpha$  agonist, we investigated whether they could induce osteogenic differentiation like estrogen<sup>37</sup>. Calcium deposits, an indication of successful osteoblast formation *in vitro*, can be specifically stained by Alizarin Red S (ARS)<sup>38</sup>. Mineralization-inducing solution induced calcium deposits in hBMSCs, which was potentially enhanced by RDNVs (20  $\mu\text{g}/\text{mL}$ , Fig. 6D). RDNVs induced significantly greater osteogenic differentiation of hBMSCs compared with the control,

which was attenuated by ICI 182,780 (fulvestrant, ER antagonist) (Fig. 6D)<sup>37</sup>. Furthermore, we investigated the underlying mechanism of RDNVs' actions in osteogenic differentiation of hBMSCs. *Runx2* is the master transcriptional factor inducing osteogenic differentiation and is induced by the classical *BMP/Smad* signaling pathway<sup>39</sup>. *BMP2*, a core *BMP* family member, plays an important role in promoting osteoblast differentiation<sup>40</sup>. Interestingly, estrogen enhanced the effects of *BMP2* on osteogenic differentiation by inducing *BMP2* gene transcription<sup>37</sup>. ER $\alpha$  up-regulation and ER $\alpha$ -induced *Runx2* and *BMP2* mRNA expression by RDNVs on Days 7 and 14 suggested that they may activate ER $\alpha$  signaling (Fig. 6E–G). Interestingly, the promotive effects of RDNVs on ER $\alpha$ -induced *Runx2* and *BMP2* activation were blocked by fulvestrant. *BMP2* is a key regulator of osteogenesis. *BMP2* regulates target genes such as *RUNX2* and *Osx* by binding to type I and type II serine/threonine kinase receptors on target cells, which in turn phosphorylate downstream Smad1/5/9. Phosphorylated Smad1/5/9 can bind to Smad4 to form complexes that translocate into the nucleus. Consistent with this, RDNVs potentially increased the protein expression levels of ER $\alpha$ , as well as of *Runx2*, *BMP2*, and Smad1/5/9, markers of osteogenic differentiation, in the induced hBMSCs. These data indicated that the *BMP2*-dependent effect of RDNVs occurred *via* activating ER $\alpha$  signaling.

### 3.6. RDNVs potentiate osteogenic differentiation of hBMSCs via ER $\alpha$ signaling

To further verify the possible mechanisms of the effective components of RDNVs, we performed a metabolomic analysis on RDNVs. Metabolomic data indicated that a total of 3075 metabolites were identified in RDNVs, including fatty acyl (15%), organic oxygen compounds (11%), carboxylic acids and their derivatives (8%), isopentenol lipids (8%), glycerophospholipids (7%), benzene and its substituted derivatives (4%), and flavonoids (3%) among others (Supporting Information Fig. S5A). The metabolites could also be classified into Super Classes, including lipids and lipid-like molecules (29%), organic oxygen compounds (10%), organic acids and their derivatives (9%), organic heterocyclic compounds (9%), phenylpropanoids and polyketides (7%), and benzene ring-type compounds (7%, Fig. S5B). It was reported that flavonoids, such as quercetin<sup>28</sup>, icariin<sup>41</sup>, and naringin<sup>42–44</sup>, were significantly correlated with pro-osteogenic properties and bone formation. Therefore, we focused on flavonoids from RDNVs.

To investigate whether the metabolites contained in RDNVs intersected with herbal Rhizoma Drynariae, we retrieved a total of 115 active ingredients of Rhizoma Drynariae through the TCMSP, TCMID, and SysMap databases. As shown in Fig. 7A, 11 common ingredients intersected between these 115 active ingredients from Rhizoma Drynariae and the metabolic components of RDNVs. The highest content of these 11 common components was of naringin, with a relative content of 6204781, which ranked first among the flavonoid and isoflavonoid metabolites and twenty-third among all RDNVs metabolites (Fig. 7B). Interestingly, the 115 effective components of Rhizoma Drynariae and 4957 osteoporosis-related genes shared a common 77 genes (Fig. 7C), and KEGG pathway analysis showed that the estrogen signaling pathway represented a major part of the shared genes (Fig. 7D). Surprisingly, the network diagram indicated that the majority of the 11 common components in RDNVs and Rhizoma Drynariae were related to core signaling targets of osteoporosis (Fig. 7E). ER $\alpha$ , as an important estrogen receptor subtype, has been widely

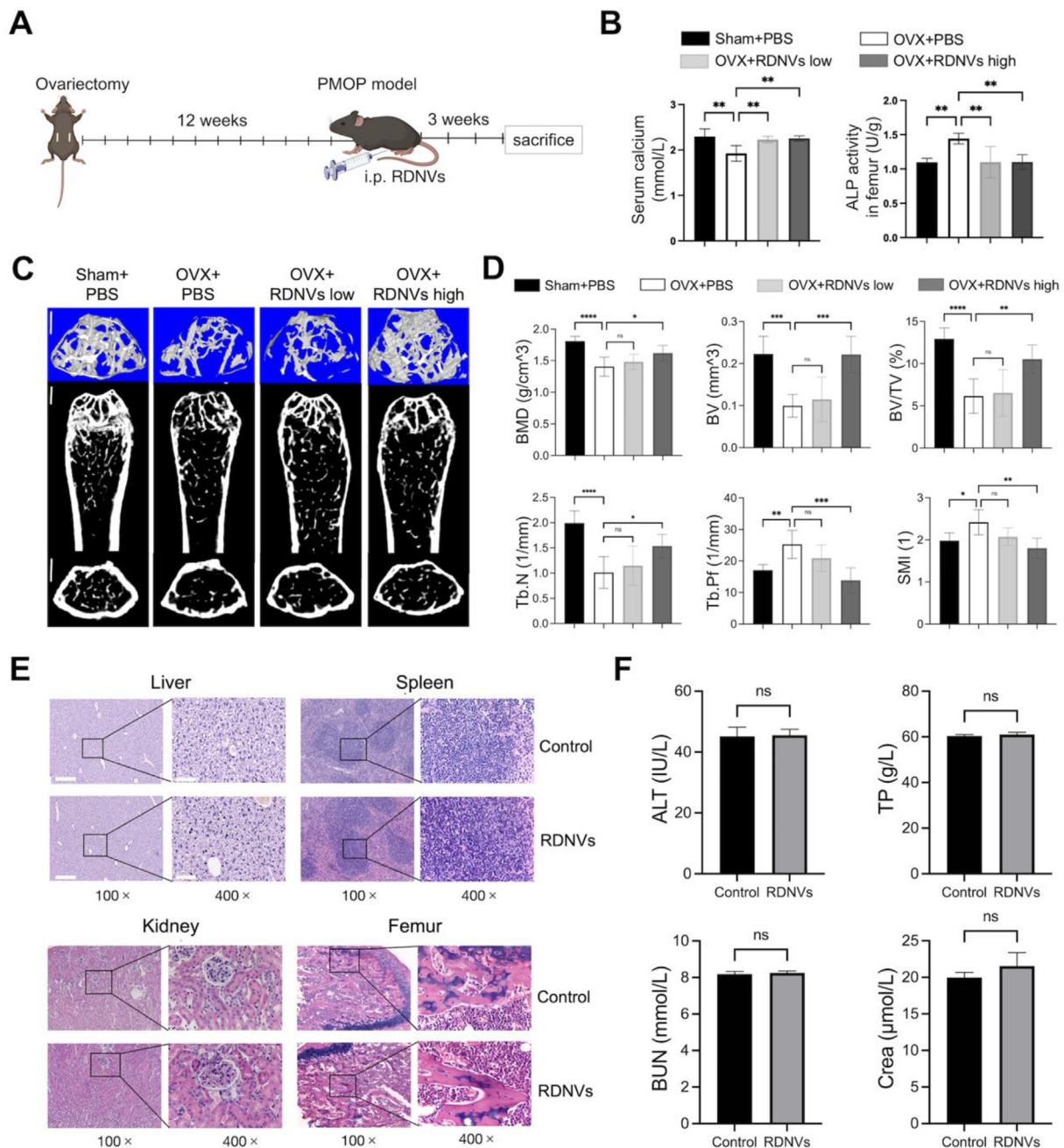


**Figure 4** RDNVs ameliorates ovariectomy-induced bone loss *in vivo*. (A) Schematic diagram of the animal experimental procedure. Female mice were subjected to bilateral ovariectomy (OVX) or sham operation (Sham). High and low concentrations of RDNVs were injected intraperitoneally for 3 weeks every other day. Mice were then sacrificed. (B) Calcium content in serum and ALP activity in femur were detected by ELISA. Data are presented as mean  $\pm$  SD ( $n = 6$ ), \*\* $P < 0.01$ . ns, not significant. (C) Mouse femurs were analyzed by micro-CT and the 3D reconstructions of trabecular were obtained using the software CTAn. Upper, three-dimensional reconstruction; Middle, sagittal; Bottom, transaxial (scale bar = 0.5 mm). (D) Histomorphometric analysis of femurs was determined by the scanner software. BMD, bone mineral density; BV, bone volume; BV/TV, bone volume density; Tb.N, trabecular number; Tb.Pf, trabecular pattern factor; SMI, structure model index. Data are presented as mean  $\pm$  SD ( $n = 6$ ), \* $P < 0.05$ , \*\* $P < 0.01$ , \*\*\* $P < 0.001$ , and \*\*\*\* $P < 0.0001$ . (E) Hematoxylin-eosin analysis of the liver, spleen, kidney, and femur from mice treated with RDNVs or PBS (as control) *via* i.p. (Scale bar: 100 $\times$ , 50  $\mu$ m; 400 $\times$ , 10  $\mu$ m). (F) The levels of liver function-related parameter (serum alanine transaminase (ALT), total protein (TP)) and kidney function-related parameters (blood urea nitrogen (BUN) and serum creatinine (Crea)) from control and RDNVs-treated mice. Data are presented as mean  $\pm$  SD ( $n = 6$ ). ns, not significant.

used as a major target of osteoporosis treatments<sup>31</sup>. Furthermore, by analysis of protein–protein interaction (PPI) networks, we found that ESR1 (ER $\alpha$ ) is one of the most vital proteins that participate in the signaling pathway of osteoporosis (Fig. 7F).

Through molecular docking, it was found that ESR1 (ER $\alpha$ ) had better binding activity to narirutin, naringin, and naringenin in RDNVs compared with other ingredients in 11 common ingredient species (the binding energy was less than  $-7$  kcal/mol). ER $\alpha$

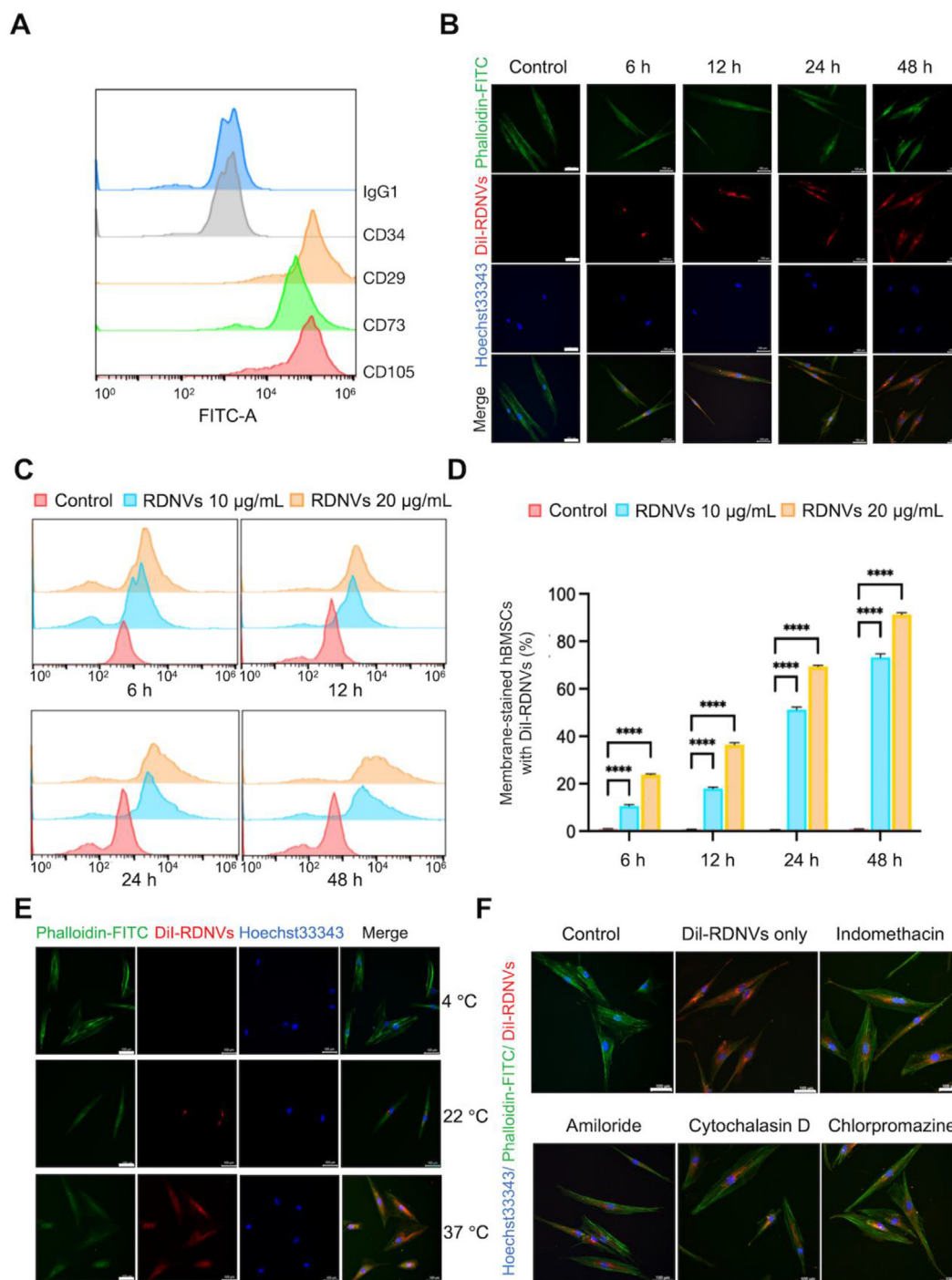


**Figure 5** Cellular uptake of RDNVs by hBMSCs *in vitro*. (A) hBMSC surface negative marker (CD34) and positive markers (CD29, CD73 and CD105) were detected by FCM analysis. (B) Representative fluorescence microscopy images of hBMSCs were treated with DiI-labeled RDNVs (20  $\mu\text{g}/\text{mL}$ ) for 6, 12, 24, and 48 h (scale bar = 100  $\mu\text{m}$ ). (C) Cellular uptake profiles of DiI-labeled RDNVs (10 and 20  $\mu\text{g}/\text{mL}$ ) in hBMSCs were detected by FCM analysis at 6, 12, 24, and 48 h, respectively. (D) Corresponding histogram of cellular uptake of DiI-labeled RDNVs in hBMSCs. Data are presented as mean  $\pm$  SD ( $n = 3$ ). \*\*\*\* $P < 0.0001$ . (E) hBMSCs were incubated with DiI-labeled RDNVs for 48 h under different temperatures (4, 22, and 37  $^{\circ}\text{C}$ ), then cells were stained and imaged by confocal microscopy. Scale bar: 100  $\mu\text{m}$ . (F) DiI-RDNVs were added after four inhibitors were incubated for one hour with hBMSCs. After 48 h, hBMSCs were coverslip-mounted with Hoechst33343 and FITC-Phalloidin for confocal imaging. Scale bar = 100  $\mu\text{m}$ .

is bonded to naringin residues ASN-439, LEU-440, GLN-441, GLU-443, TRP-393, and GLU-397, which contributes to the stability of the structure (Fig. 7G). To prove that Naringin has a binding relationship with ER $\alpha$  (ESR1), surface plasmon resonance

(SPR) and drug affinity responsive target stability (DARTS) assay were conducted. The SPR results reveal that the binding and dissociation of Naringin to human ER $\alpha$  showed a clear concentration dependence and time-dependence, characteristic of slow

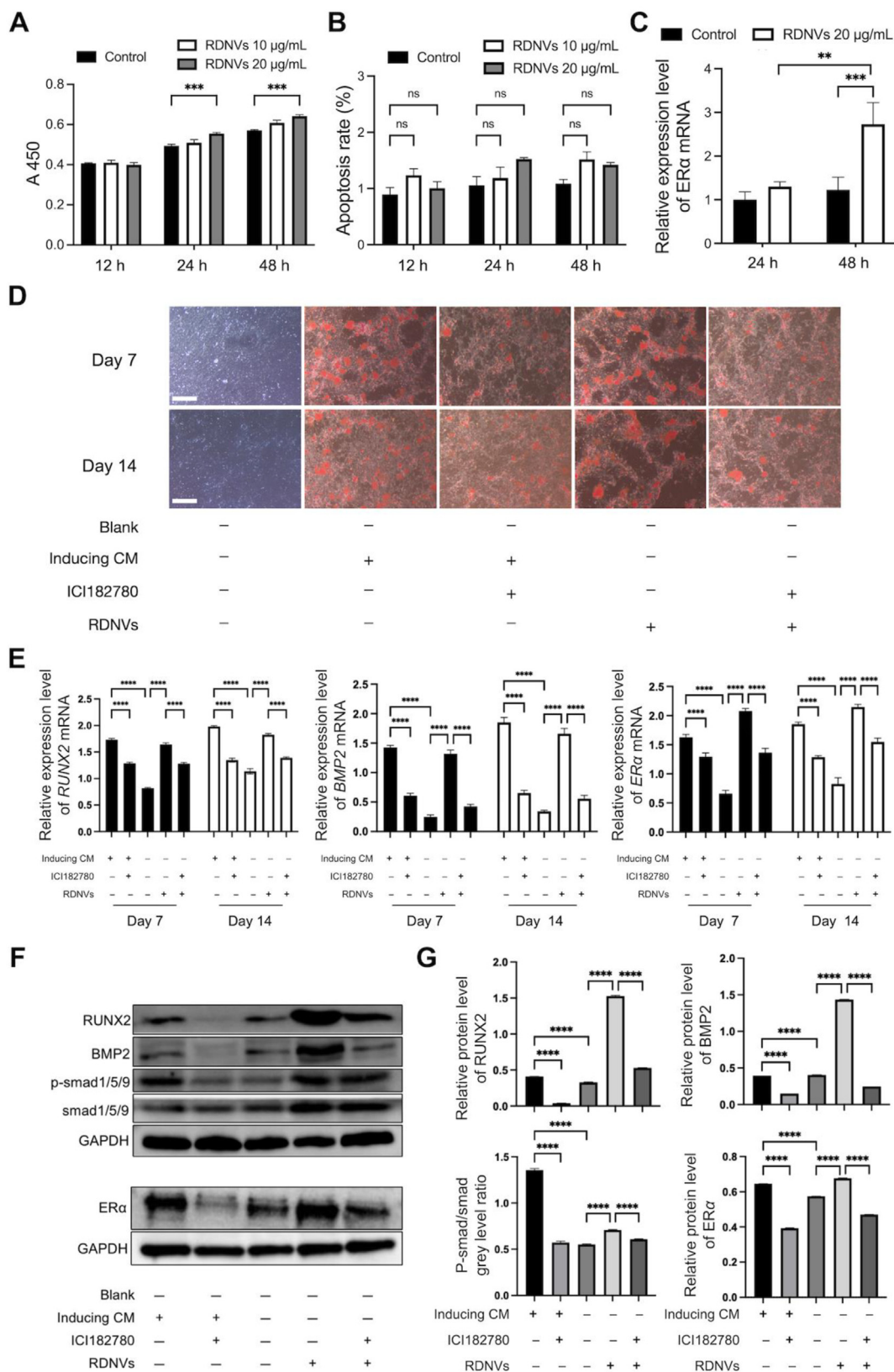


**Figure 6** RDNVs promote hBMSC proliferation and differentiation *in vitro*. (A) Pro-proliferative capacities of RDNVs (0, 10 and 20  $\mu\text{g/mL}$ ) against hBMSCs after co-incubation for 12, 24, and 48 h, respectively, were detected by CCK8 assay. (B) Apoptosis of hBMSCs on treatment with RDNVs (0, 10 and 20  $\mu\text{g/mL}$ ) for 12, 24, and 48 h were determined by FCM. (C) ER $\alpha$  mRNA expression levels during hBMSC proliferation after co-incubating with RDNVs (20  $\mu\text{g/mL}$ ) for 24 or 48 h were determined by PCR. (D) ARS images of hBMSCs on Days 7 and 14 of osteogenic differentiation (scale bar = 20  $\mu\text{m}$ ). (E) Effect of RDNVs on osteogenesis-related markers and ER $\alpha$  mRNA levels in hBMSCs on Days 7 and 14

dissociation, suggesting that they could bind specifically (Fig. 7H). The DARTS results show that ER $\alpha$  can be stabilized after binding with Naringin so that it can resist the digestion of the Thermolysin. ER $\alpha$  protein incubated with naringin has a distinct band at about 70 kDa, and Naringin can protect the protein in this band against the digestive action of Thermolysin. When different concentrations of Thermolysin digested the target protein ER $\alpha$ , Naringin reduced the digestion effect to different degrees. Therefore, ER $\alpha$  in this band is considered to be a possible binding target of Naringin (Fig. 7I).

#### 4. Discussion

To date, large numbers of nanomedicine platforms, including synthesized nanoparticles and NVs from mammalian cells, have been demonstrated to be effective in treating various diseases<sup>11,45,46</sup>. However, due to limited therapeutic outcomes, potential side reactions, and possible *in vivo* biotoxicity of artificial nanoparticles, few of them have been approved by regulatory agencies for clinical translation<sup>47,48</sup>. Compared to artificial nanoparticles, NVs from mammalian cells display other benefits, such as low biotoxicity and specific tissue-targeting activities<sup>49,50</sup>. Nonetheless, the therapeutic application of mammalian-derived NVs is challenging due to underlying biological hazard risks for humans and achieving large-scale economic production<sup>51</sup>. Recently, natural plant-derived NVs have been extracted from various fresh herbs (*e.g.*, ginseng, turmeric, and mulberry bark), which displayed therapeutic immunomodulatory effects in colitis<sup>35,49,52</sup>. They independently demonstrated herb-derived NVs to be safe, act as multi-functional platforms, and can be scaled up for mass production. However, a role in the treatment of osteoporosis is lacking.

In particular, we focused on Rhizoma Drynariae, which is well-known for its multiple pharmacological properties, including bone strengthening, anti-pain, and anti-osteoporosis, and is widely used as a medicinal herb or a dietary supplement<sup>21,53,54</sup>. As reported, flavones from plants could exert promotional functions on osteogenic differentiation and bone formation<sup>22,28,42</sup>. In the study, we hypothesized that RDNVs extracted from Rhizoma Drynariae root, containing large amounts of flavones, could be used to treat PMOP. TEM, nFCM and Zeta potential analyses indicated that RDNVs, isolated by ultracentrifugation, had a typical morphology and particle size similar to those of mammalian-derived NVs (Fig. 2A–D). Moreover, the yield of RDNVs, reaching 20  $\mu$ g protein per gram Rhizoma Drynariae, was higher than those of NVs from mammalian cells. Furthermore, with high purity and concentration, RDNVs also contained bioactive components such as proteins, lipids, and nucleic acids (Fig. 2E–G).

The experiments *in vivo* revealed that RDNVs could efficiently target the femur and promote bone formation (Figs. 3 and 4). It is of note that intraperitoneally administered RDNVs achieved comparable target effects to intravenous RDNVs injection. These findings indicated that RDNVs *via* i.p. administration could be absorbed into the circulatory system. Interestingly, we found that RDNVs specifically targeted mBMSCs but not PBMCs, which indicated the possible bone-specific effects of RDNVs. Furthermore, by analyzing representative micro-CT images and bone

histomorphometric parameters of femurs, we demonstrated that RDNVs are efficient nanoplatforms that improve bone mass and quality for further anti-osteoporosis activities (Fig. 4B–D).

Subsequently, we demonstrated that RDNVs could be internalized by hBMSCs with high efficiency. It was reported that Dil-labeled ginseng-derived nanoparticles were internalized by mouse bone marrow-derived macrophages (BMDMs) after co-incubation for 12 h, and the uptake percentage of mouse BMDMs containing these nanoparticles increased with time from 41.3% at 12 h to 57.4% at 24 h<sup>26</sup>. In our study, the cellular uptake percentages of Dil-RDNVs by hBMSCs increased in a concentration- and time-dependent manner (Fig. 5B–D). The higher cell internalization rate of RDNVs might be attributed to their surface-specific contents, which could efficiently mediate the interaction with hBMSCs.

Additionally, we revealed the anti-osteoporosis mechanism of RDNVs, and their capacity to promote osteogenic differentiation was mainly dependent on the induction of increased key osteogenic mRNA and protein levels in hBMSCs (Fig. 6). Our experiments indicated that RDNVs stimulated hBMSC proliferation at the early stage (Fig. 6A). It was previously reported that treatment with the ER $\alpha$  inhibitor ICI 182,780 blocks the effects of quercetin, a flavonoid that promotes hBMSC proliferation and osteogenic differentiation<sup>28</sup>. Considering that naringin is a flavonoid, we further analyzed the proliferation and osteogenic differentiation of hBMSCs in response to RDNVs. Similar to the induced culture medium, treatment with RDNVs substantially stimulated osteogenic differentiation, while ICI 182,780 (ER antagonist) attenuated this process, which suggested that ER is an important signaling receptor for RDNVs (Fig. 6C). Flavonoids are chemically similar to estrogen<sup>36</sup>. Recent studies have shown that estrogen upregulates BMP2 gene transcription and enhances the activation of the BMP signaling pathway (BMP2/Smad/RUNX2), thereby promoting osteogenesis<sup>37,55</sup>. RDNVs treatment upregulated the BMP2 expression level in hBMSCs, triggering the expression of osteogenic differentiation-related genes, such as RUNX2 (Fig. 6D). Moreover, RDNV treatment significantly upregulated ER $\alpha$  and osteogenic differentiation-related protein expression of hBMSCs, which was diminished by ICI 182,780 (Fig. 6E). Taken together, these results proved that the osteoinductive efficacy of RDNVs indicated its ability to accelerate osteogenesis through vigorously stimulating hBMSCs proliferation and osteogenic differentiation. To further elucidate the mechanisms by which RDNVs display bone-formation effects, particularly in stimulating hBMSCs osteogenic differentiation, metabolomic analysis was conducted. It was reported that the metabolites 6-shogaol from ginger-derived NVs or sulforaphane from broccoli-derived NVs play an important role in the prevention of alcohol-induced liver damage and colitis, respectively<sup>19,56</sup>. Our data showed that RDNVs and Rhizoma Drynariae shared 11 common metabolic substances, of which naringin had the highest average expression level (Fig. 7A and B). Naringin is a flavonoid glycoside with pro-osteogenic, antiresorptive, and antiadipogenic properties, which can promote hBMSCs proliferation and osteogenic differentiation<sup>21,43,44</sup>. In addition, we found that narirutin, naringin, and naringenin were the three most effective substances in binding to the ER $\alpha$  by molecular docking screening (Fig. 7G–

of osteogenesis differentiation was determined by PCR. (F, G) Effect of RDNVs on osteogenesis-related markers and ER $\alpha$  protein levels in hBMSCs on Day 14 of osteogenesis differentiation was detected by Western blot. Data are presented as mean  $\pm$  SD ( $n = 3$ ). \* $P < 0.05$ , \*\* $P < 0.01$ , \*\*\* $P < 0.001$  and \*\*\*\* $P < 0.0001$ . ns, no significant.

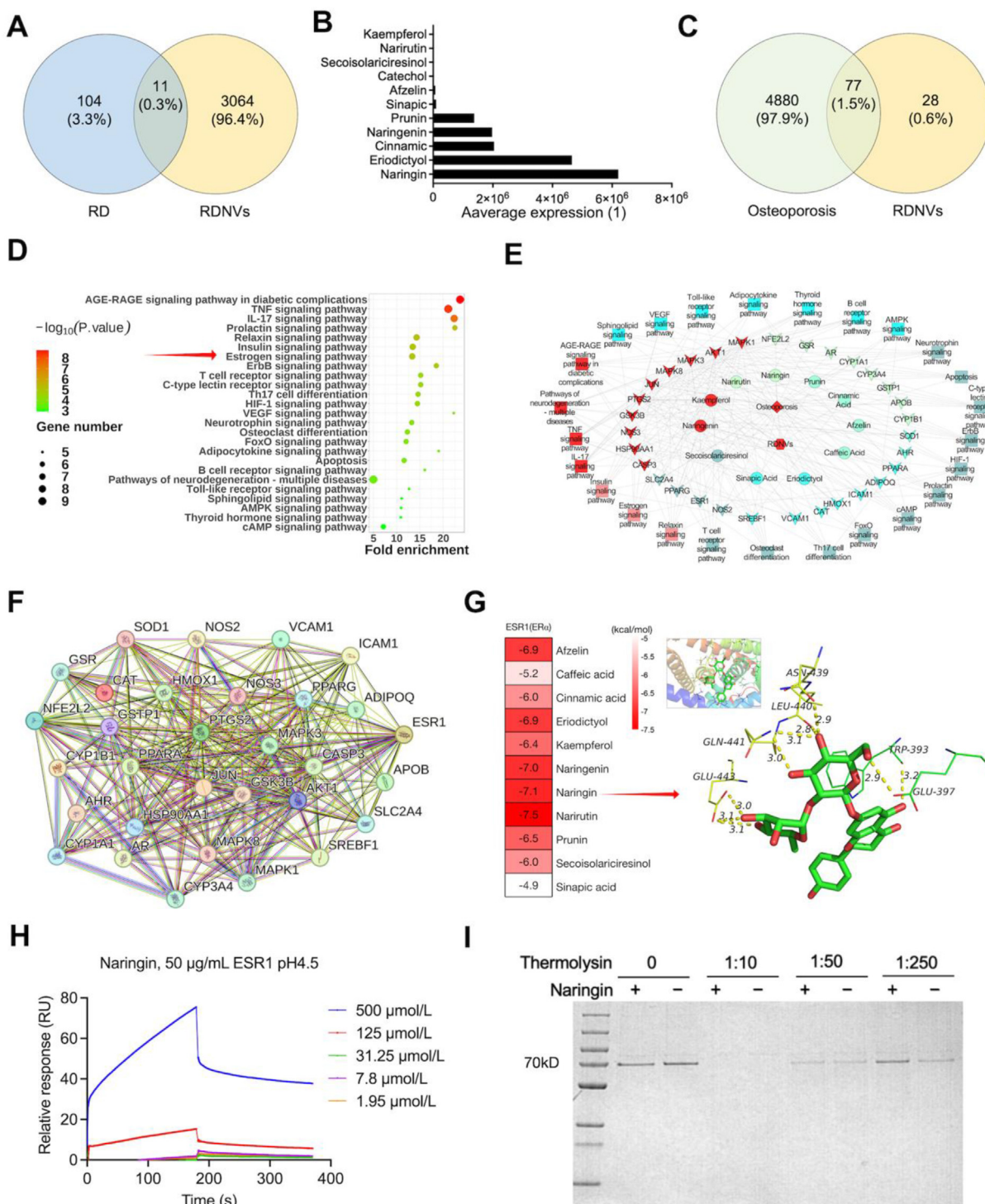


**Figure 7** RDNVs exert effects on alleviating bone loss *via* ER $\alpha$  signaling. (A) Venn diagram and (B) ranking of the 11 most common components of the metabolites intersection of RDNVs and Rhizoma Drynariae. (C) Venn diagram and (D) KEGG pathway analysis of 77 common components of the intersection of RDNVs and osteoporosis genes. (E) Network diagram of 11 common intersected components between RDNVs and Rhizoma Drynariae and signaling pathways related to core targets of osteoporosis. (F) PPI network of 11 common components on osteoporosis. (G) Binding energy heatmap of molecular docking for 11 consensus components and cartoon model plot of molecular docking of naringin, naringenin, and narirutin with ER $\alpha$ . (H) Naringin and ER $\alpha$  affinity assay (SPR method). (I) Naringin and ER $\alpha$  affinity assay (DARTS method). The changes of ER $\alpha$  protein after incubation with Naringin and Thermolysin at different concentrations (Thermolysin: ER $\alpha$  protein ratios: 1:10, 1:50, 1:250) were detected by SDS-PAGE.

D). Moreover, HPLC confirmed that Naringin, the main active ingredient, exists in RDNVs. Whether it plays a vital role in anti-PMOP is something we will continue to explore.

The current study represents a preliminary investigation for research and application of Chinese herbal medicine derived EVs<sup>57</sup>. RDNVs, which act as messengers mediating intercellular communication and regulate pathophysiological processes *in vivo*, may be a suitable candidate for future anti-osteoporosis drugs. However, there are some limitations to our study. The mechanism that naringin could be easier to enter into BMSCs and bind with ER $\alpha$  in RDNVs is unclear. It has been shown that the basic properties of EVs can be used to “modify” the recipient cell by delivering membrane proteins to the recipient cell membrane through membrane fusion. These proteins are then “inserted” into the receptor cell membrane and can be used as targets for targeted therapies. This novel approach represents a facile method of altering cell membrane antigen presentation *via* convenient EVs uptake and may pave the way for the burgeoning wave of targeted therapy and/or immunotherapy<sup>56</sup>. Therefore, it is the direction we want to explore further subsequently.

## 5. Conclusions

In this study, we demonstrated that the natural product RDNVs, isolated and purified from fresh *Rhizoma Drynariae*, was a high-efficacy agonist of ER $\alpha$  and a potential nano-drug platform for the prevention and treatment of PMOP (Fig. 1). Furthermore, *in vivo* experiments indicated that RDNVs preferentially accumulated in femur tissues, and the bioactive component naringin increased the bone mass and contributed to an anti-PMOP response. Moreover, we revealed the underlying mechanism of the pro-osteogenic properties of naringin enriched in RDNVs *via* targeting of ER $\alpha$  signaling. This study contributes to the development of a novel nanotherapeutic platform for the treatment of PMOP *via* i.p. administration, which has a promising potential for clinical translation.

## Acknowledgments

This work was supported by the National Natural Science Foundation of China (Nos. 82174119, 81973633 and 82274220), Science and Technology Projects in Liwan District, Guangzhou (Nos. 20230710 and 202201009, China), Young Talent Support Project of Guangzhou Association for Science and Technology (No. QT2023036, China), Special focus areas for General Universities in Guangdong Province (No. 2022ZDZX2016, China), Guangdong Provincial Administration of Traditional Chinese Medicine Project (No. 20233025, China).

## Author contributions

Ke-wei Zhao and Qing Zhao designed the research, provided funding acquisition, and methodology. Qing Zhao, Jun-jie Feng, and Fu-bin Liu wrote the original manuscript. Qing Zhao revised the manuscript. Qian-xin Liang, Man-lin Xie, Jia-ming Dong, Yan-fang Zou, and Jia-li Ye carried out the experiments and performed data analysis. Gui-long Liu, Yue Cao, and Zhao-di Guo participated in part of the experiments. Lei Zheng and Hong-zhi Qiao provided methodology and resources. All of the authors have read and approved the final manuscript.

## Conflicts of interest

The authors have no conflicts of interest to declare.

## Appendix A. Supporting information

Supporting data to this article can be found online at <https://doi.org/10.1016/j.apsb.2024.02.005>.

## References

- Khosla S, Oursler MJ, Monroe DG. Estrogen and the skeleton. *Trends Endocrinol Metab* 2012;**23**:576–81.
- Watts NB. Postmenopausal osteoporosis: a clinical review. *J Womens Health (Larchmt)* 2018;**27**:1093–6.
- Arron JR, Choi Y. Bone versus immune system. *Nature* 2000;**408**:535–6.
- Phan TC, Xu J, Zheng MH. Interaction between osteoblast and osteoclast: impact in bone disease. *Histol Histopathol* 2004;**19**:1325–44.
- Corsi A, Ungari C, Riminucci M, Agrillo A. Bisphosphonate-related osteonecrosis and metastasis within the same site of the jaw. *J Oral Maxillofac Surg* 2017;**75**:1679–84.
- Herrero S, Pico Y. Treatments for post-menopausal osteoporotic women, what's new? how can we manage long-term treatment?. *Eur J Pharmacol* 2016;**779**:8–21.
- Gambacciani M, Levancini M. Hormone replacement therapy and the prevention of postmenopausal osteoporosis. *Prz Menopauzalny* 2014;**4**:213–20.
- Rossouw JE, Anderson GL, Prentice RL, LaCroix AZ, Kooperberg C, Stefanick ML, et al. Risks and benefits of estrogen plus progestin in healthy postmenopausal women: principal results from the Women's Health Initiative randomized controlled trial. *JAMA* 2002;**288**:321–33.
- Colombo M, Raposo G, Théry C. Biogenesis, secretion, and intercellular interactions of exosomes and other extracellular vesicles. *Annu Rev Cell Dev Biol* 2014;**30**:255–89.
- Tkach M, Théry C. Communication by extracellular vesicles: where we are and where we need to go. *Cell* 2016;**164**:1226–32.
- EL Andaloussi S, Mäger I, Breakefield XO, Wood MJA. Extracellular vesicles: biology and emerging therapeutic opportunities. *Nat Rev Drug Discov* 2013;**12**:347–57.
- Jung KO, Jo HH, Yu JH, Gambhir SS, Pratz G. Development and MPI tracking of novel hypoxia-targeted theranostic exosomes. *Biomaterials* 2018;**177**:139–48.
- Li WY, Liu YS, Zhang P, Tang YM, Zhou M, Jiang WR, et al. Tissue-engineered bone immobilized with human adipose stem cells-derived exosomes promotes bone regeneration. *ACS Appl Mater Interfaces* 2018;**10**:5240–54.
- Zhang MZ, Viennois E, Prasad M, Zhang YC, Wang LX, Zhang Z, et al. Edible ginger-derived nanoparticles: a novel therapeutic approach for the prevention and treatment of inflammatory bowel disease and colitis-associated cancer. *Biomaterials* 2016;**101**:321–40.
- Dad HA, Gu TW, Zhu AQ, Huang LQ, Peng LH. Plant exosome-like nanovesicles: emerging therapeutics and drug delivery nanoplatfoms. *Mol Ther* 2021;**29**:13–31.
- Rutter BD, Innes RW. Extracellular vesicles isolated from the leaf apoplast carry stress-response proteins. *Plant Physiol* 2017;**173**:728–41.
- Cai Q, Qiao LL, Wang M, He BY, Lin FM, Palmquist J, et al. Plants send small RNAs in extracellular vesicles to fungal pathogen to silence virulence genes. *Science* 2018;**360**:1126–9.
- Teng Y, Ren Y, Sayed M, Hu X, Lei C, Kumar A, et al. Plant-derived exosomal microRNAs shape the gut microbiota. *Cell Host Microbe* 2018;**24**:637–52.

19. Zhuang XY, Deng ZB, Mu JY, Zhang LF, Yan J, Miller D, et al. Ginger-derived nanoparticles protect against alcohol-induced liver damage. *J Extracell Vesicles* 2015;**4**:28713.
20. Wang QL, Ren Y, Mu JJ, Egilmez NK, Zhuang XY, Deng ZB, et al. Grapefruit-derived nanovectors use an activated leukocyte trafficking pathway to deliver therapeutic agents to inflammatory tumor sites. *Cancer Res* 2015;**75**:2520–9.
21. Zhang P, Dai KR, Yan SG, Yan WQ, Zhang C, Chen D, et al. Effects of naringin on the proliferation and osteogenic differentiation of human bone mesenchymal stem cell. *Eur J Pharmacol* 2009;**607**:1–5.
22. Song SH, Gao ZY, Lei XJ, Niu YB, Zhang Y, Li CQ, et al. Total flavonoids of *Drynariae rhizoma* prevent bone loss induced by hindlimb unloading in rats. *Molecules* 2017;**22**:1033.
23. Abdifetah O, Na-Bangchang K. Pharmacokinetic studies of nanoparticles as a delivery system for conventional drugs and herb-derived compounds for cancer therapy: a systematic review. *Int J Nanomedicine* 2019;**14**:5659–77.
24. Wan SB, Yang H, Zhou Z, Cui QC, Chen D, Kanwar J, et al. Evaluation of curcumin acetates and amino acid conjugates as proteasome inhibitors. *Int J Mol Med* 2010;**26**:447–55.
25. Cao M, Yan HJ, Han X, Weng L, Wei Q, Sun XY, et al. Ginseng-derived nanoparticles alter macrophage polarization to inhibit melanoma growth. *J Immunotherapy Cancer* 2019;**7**:326.
26. Cao Y, Zhao Q, Liu FB, Zheng L, Lin XD, Pan MY, et al. Drug value of *Drynariae Rhizoma* root-derived extracellular vesicles for neurodegenerative diseases based on proteomics and bioinformatics. *Plant Signal Behav* 2022;**17**:2129290.
27. Chen QB, Li Q, Liang YQ, Zu MH, Chen NX, Canup BSB, et al. Natural exosome-like nanovesicles from edible tea flowers suppress metastatic breast cancer via ROS generation and microbiota modulation. *Acta Pharm Sin B* 2022;**12**:907–23.
28. Pang XG, Cong Y, Bao NR, Li YG, Zhao JN. Quercetin stimulates bone marrow mesenchymal stem cell differentiation through an estrogen receptor-mediated pathway. *BioMed Res Int* 2018;**15**:1–11.
29. Strong AL, Ohlstein JF, Jiang Q, Zhang Q, Zheng S, Boue SM, et al. Novel daidzein analogs enhance osteogenic activity of bone marrow-derived mesenchymal stem cells and adipose-derived stromal/stem cells through estrogen receptor dependent and independent mechanisms. *Stem Cell Res Ther* 2014;**5**:105.
30. Zhou J, Zhang ZY, Joseph J, Zhang XC, Ferdows BE, Patel DN, et al. Biomaterials and nanomedicine for bone regeneration: progress and future prospects. *Exploration* 2021;**1**:20210011.
31. Smiley D, Khalil R. Estrogenic compounds, estrogen receptors and vascular cell signaling in the aging blood vessels. *Curr Med Chem* 2009;**16**:1863–87.
32. Ilaibaks NF, Lei ZY, Mol EA, Deshantri AK, Jiang LL, Schiffelers RM, et al. Biofabrication of cell-derived nanovesicles: a potential alternative to extracellular vesicles for regenerative medicine. *Cells* 2019;**8**:1509.
33. Wiklander OP, Nordin JZ, O'Loughlin A, Gustafsson Y, Corso G, Mäger I, et al. Extracellular vesicle *in vivo* biodistribution is determined by cell source, route of administration and targeting. *J Extracell Vesicles* 2015;**20**:26316.
34. Wang YY, Yao J, Cai LZ, Liu T, Wang XG, Zhang Y, et al. Bone-targeted extracellular vesicles from mesenchymal stem cells for osteoporosis therapy. *Int J Nanomedicine* 2020;**15**:7967–77.
35. Liu C, Yan XJ, Zhang YJ, Yang M, Ma YN, Zhang YY, et al. Oral administration of turmeric-derived exosome-like nanovesicles with anti-inflammatory and pro-resolving bioactions for murine colitis therapy. *J Nanobiotechnology* 2022;**20**:206.
36. Zhang ND, Han T, Huang BK, Rahman K, Jiang YP, Xu HT, et al. Traditional Chinese medicine formulas for the treatment of osteoporosis: implication for antiosteoporotic drug discovery. *J Ethnopharmacol* 2016;**189**:61–80.
37. Matsumoto Y, Otsuka F, Takano M, Mukai T, Yamanaka R, Takeda M, et al. Estrogen and glucocorticoid regulate osteoblast differentiation through the interaction of bone morphogenetic protein-2 and tumor necrosis factor-alpha in C2C12 cells. *Mol Cell Endocrinol* 2010;**325**:118–27.
38. Zakhireh S, Adibkia K, Beygi-Khosrowshahi Y, Barzegar-Jalali M. Osteogenesis promotion of selenium-doped hydroxyapatite for application as bone scaffold. *Biol Trace Elem Res* 2021;**199**:1802–11.
39. Sautchuk R, Kalicharan BH, Escalera-Rivera K, Jonason JH, Porter GA, Awad HA, et al. Transcriptional regulation of cyclophilin D by BMP/Smad signaling and its role in osteogenic differentiation. *Elife* 2022;**11**:e75023.
40. Zhou N, Li Q, Lin X, Hu N, Liao JY, Lin LB, et al. BMP2 induces chondrogenic differentiation, osteogenic differentiation and endochondral ossification in stem cells. *Cell Tissue Res* 2016;**366**:101–11.
41. Zhang DW, Fong CC, Jia ZB, Cui L, Yao XS, Yang MS. Icaritin stimulates differentiation and suppresses adipocytic trans-differentiation of primary osteoblasts through estrogen receptor-mediated pathway. *Calcif Tissue Int* 2016;**99**:187–98.
42. Lavrador P, Gaspar VM, Mano JF. Bioinspired naringin-loaded micelles for guiding stem cell osteodifferentiation. *Adv Healthcare Mater* 2018;**7**:1800890.
43. Wang HC, Li CB, Li JM, Zhu YJ, Jia YD, Zhang Y, et al. Naringin enhances osteogenic differentiation through the activation of ERK signaling in human bone marrow mesenchymal stem cells. *Iran J Basic Med Sci* 2017;**20**:408–14.
44. Lavrador P, Gaspar VM, Mano JF. Bioinspired bone therapies using naringin: applications and advances. *Drug Discov Today* 2018;**23**:1293–304.
45. Chen QB, Ma Y, Bai P, Li Q, Canup BSB, Long DP, et al. Tumor microenvironment-responsive nanococktails for synergistic enhancement of cancer treatment via cascade reactions. *ACS Appl Mater Interfaces* 2021;**13**:4861–73.
46. Zhang XQ, Huang YM, Song HL, Canup BSB, Gou SQ, She ZG, et al. Inhibition of growth and lung metastasis of breast cancer by tumor-homing triple-bioresponsive nanotherapeutics. *J Control Release* 2020;**328**:454–69.
47. Dancy JG, Wadajkar AS, Connolly NP, Galisteo R, Ames HM, Peng S, et al. Decreased nonspecific adhesivity, receptor-targeted therapeutic nanoparticles for primary and metastatic breast cancer. *Sci Adv* 2020;**6**:eaax3931.
48. Landgraf M, Lahr CA, Kaur I, Shafiee A, Sanchez-Herrero A, Janowicz PW, et al. Targeted camptothecin delivery via silicon nanoparticles reduces breast cancer metastasis. *Biomaterials* 2020;**240**:119791.
49. Pi FM, Binzel DW, Lee TJ, Li ZF, Sun MY, Rychahou P, et al. Nanoparticle orientation to control RNA loading and ligand display on extracellular vesicles for cancer regression. *Nat Nanotechnol* 2018;**13**:82–9.
50. Zhang W, Yu ZL, Wu M, Ren JG, Xia HF, Sa GL, et al. Magnetic and folate functionalization enables rapid isolation and enhanced tumor-targeting of cell-derived microvesicles. *ACS Nano* 2017;**11**:277–90.
51. Wang QL, Zhuang XY, Mu JY, Deng ZB, Jiang H, Zhang LF, et al. Delivery of therapeutic agents by nanoparticles made of grapefruit-derived lipids. *Nat Commun* 2013;**4**:1867.
52. Sriwastva MK, Deng ZB, Wang BM, Teng Y, Kumar A, Sundaram K, et al. Exosome-like nanoparticles from Mulberry bark prevent DSS-induced colitis via the AhR/COPS8 pathway. *EMBO Rep* 2022;**23**:53365.
53. Gan DH, Xu XW, Chen DQ, Feng P, Xu ZW. Network pharmacology-based pharmacological mechanism of the Chinese medicine *Rhizoma drynariae* against osteoporosis. *Med Sci Monit* 2019;**25**:5700–16.

54. Lin J, Zhu J, Wang Y, Zhang N, Gober HJ, Qiu XM, et al. Chinese single herbs and active ingredients for postmenopausal osteoporosis: from preclinical evidence to action mechanism. *Biosci Trends* 2017;**11**:496–506.
55. Lin GL, Hankenson KD. Integration of BMP, Wnt, and notch signaling pathways in osteoblast differentiation. *J Cell Biochem* 2011;**112**:3491–501.
56. Deng ZB, Rong Y, Teng Y, Mu JY, Zhuang XY, Tseng M, et al. Broccoli-derived nanoparticle inhibits mouse colitis by activating dendritic cell AMP-activated protein kinase. *Molr Ther* 2017;**25**:1641–54.
57. Zhao Q, Wang T, Wang HB, Cao P, Jiang CY, Qiao HZ, et al. Consensus statement on research and application of Chinese herbal medicine derived extracellular vesicles-like particles (2023 edition). *Chinese Herb Med* 2024;**16**:3–12.